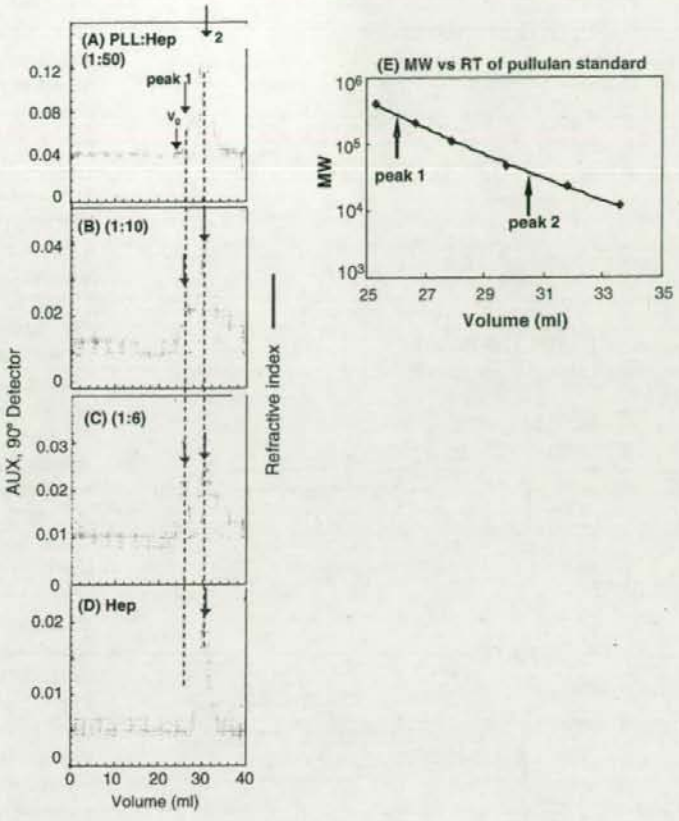

Fig 1 Elution of BPL-Hep probe by SEC-MALLS. BPL-Hep probes were prepared from the materials in the molar ratios PLL:Hep=1:6 (**a**), 1:10 (**b**), 1:50 (**c**), and were injected on a Dawn DSP HPLC system of SEC and detected by MALLS and refractive index (RI), as described in the text. Underivatized free heparin was injected as a control (**d**). The elution patterns detected by MALLS are expressed as *dots*, and those of RI are expressed as *solid lines*

respectively. The bulk effect changes in RU induced by binding of the analytes to the probe-immobilized flow cell were corrected by subtracting the changes of the respective control flow cells. This correction removed the interference by non-specific binding of the analytes to the backbone PLL or biotin moiety of the probes at the same time. AT-III, thrombin, and lactoferrin concentration-dependently bound to BPL-Hep (Fig. 2) and biotin-hydrazide-Hep, but they did not bind to BPL and biotin (data not shown). The association rate constant (k_a), dissociation rate constant (k_d), and dissociation constant (K_d) were calculated and are summarized in Table 1. Among the samples, β-lactoferrin bound best to the BPL-Hep-immobilized flow cell with a K_d of 1.2×10^{-9} M^{-1}, which is 40-fold lower than the K_d of biotin-hydrazide-Hep, 4.4×10^{-8} M^{-1}. Thrombin bound to the immobilized BPL-Hep at a K_d that was threefold lower than the K_d of biotin-hydrazide-Hep. While AT-III showed considerable binding to BPL-Hep, it bound very little to biotin-hydrazide-Hep, and the fitting to calculate the parameters was low. The low k_{ds} of BPL-Hep to β-lactoferrin and AT-III indicate that the bound β-lactoferrin and AT-III only slowly dissociate from the BPL-Hep probe, which caused the high affinity of pseudoPG. These results indicate that the heparin-binding proteins examined showed remarkably higher affinity to the Hep-pseudoPG probe than that to the single-chain heparin probe.

Membrane detection of GAG-binding proteins To examine whether the binding specificity depends on the glycan moiety or skeletal polymer, pseudoPG probes containing various GAGs were applied to the detection of binding proteins in brain extract from rats that had been denatured by SDS-PAGE and electroblotted onto a PVDF membrane. As shown in Fig. 3, each probe showed differential binding to many proteins. The BPL-Hep probe bound to several bands distinct from those of the biotin hydrazide-Hep probe, except that some proteins commonly bound to both probes. The BPL-Hep probe showed higher staining intensity at the same heparin concentration, probably because it had higher affinity in addition to a higher biotin concentration than the biotin-hydrazide-Hep probe. BPL-

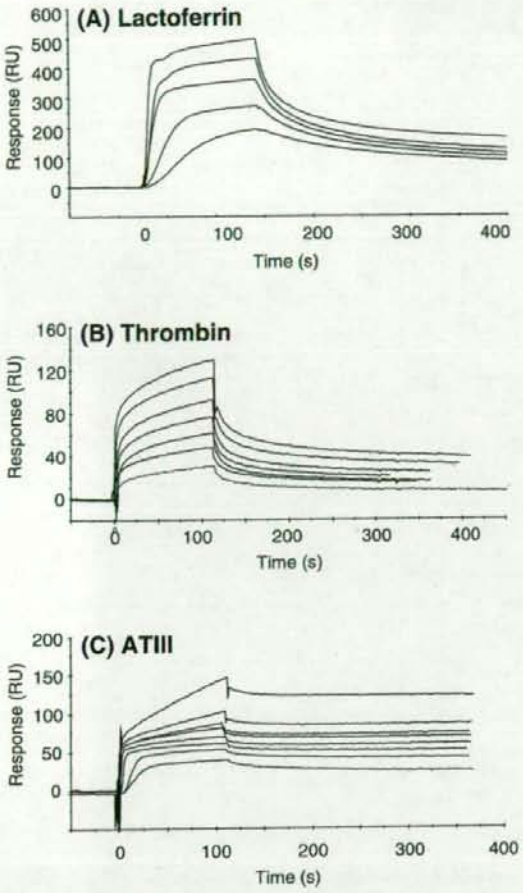

Fig 2 Quantification of interaction between Hep-BPL and Hep-binding proteins by SPR. Hep-BPL was immobilized on a CM5 sensor chip as described in the text. Plasma glycoproteins were serially diluted twofold and injected onto a Hep-BPL-immobilized sensor chip in 10 mM HB-EPS (pH 7.5) for 150 s at a flow rate of 20 μl/min at 25°C. The response was expressed as the change in resonance units (RU) induced by binding of the protein to the Hep-BPL immobilized flow cell, which was corrected for bulk effect by subtracting the change on the BPL-immobilized reference cell. Binding curves of various concentrations of glycoproteins on the sensor chip were 11.9–190 nM lactoferrin (**a**), 0.42–27.0 μM thrombin (**b**), and 0.26–17.4 μM AT-III (**c**)

chondroitin sulfates A and B and BPL-colominic acid probes showed similar binding patterns, which were quite different from those of Hep probes and the BPL-glucuronic acid probe. Only endogenous avidin was detected with a control BPL probe, at a position corresponding to 68 kDa, indicating that BPL did not bind to any of the proteins on the membrane. Essentially the same reactivity was observed between the heparin pseudoPGs of different skeletal polymers, BPL-Hep and BPA-Hep.

Identification of pseudoPG-binding proteins by affinity chromatography The binding specificities of pseudoPG for native proteins were compared by affinity chromatography using the immobilized Hep-PLL, Hep-PLL-Sepharose, and a heparin adsorbent prepared by the conventional condensation method, Hep-Sepharose. An *N*-acetylated PLL-Sepharose or Sepharose column was used as a precolumn for the Hep-PLL-Sepharose and Hep-Sepharose columns, respectively, to remove nonspecific binding of each adsorbent caused by the PLL moiety and Sepharose matrix. Therefore, the differences in the proteins that bound to Hep-PLL-Sepharose from those that bound to heparin-Sepharose are attributable to the binding to the PG structure. The rat brain extract was applied to the columns, and the bound proteins were eluted with increasing concentrations of NaCl. As shown in Fig. 4, the proteins eluted with 0.5 M NaCl showed different patterns between the columns on SDS-PAGE (Fig. 4c), while the proteins were scarcely observed in the 2 M NaCl fractions.

The proteins that specifically bound to either of the two adsorbents were identified by direct N-terminal sequencing of each protein on the excised PVDF membrane, and they are summarized in Fig. 4d. Among the proteins that specifically bound to the Hep-PLL-Sepharose column, band 'c' (18 kDa) was identified as a small immunophilin, CypA. The N-terminal sequences of band 'd' (95 kDa) and band 'e' (96 kDa) coincided with those of heat-shock proteins, HSP90α and HSP90β, respectively. Band 'b' was N-terminally blocked. The 32 kDa protein N-terminal sequence (band a) that bound to Hep-Sepharose was identified as a neurite-promoting factor, amphoterin (HMG1).

The affinity chromatography was also carried out for a normal porcine brain extract eluted with 0.5 M NaCl (Fig. 5). As shown in Fig. 5c, the anti-CypA antibody strongly bound to the 18-kDa band in lane 4, and the binding to the band was completely inhibited by recombinant human CypA (data not shown). Therefore, CypA was more enriched in the fraction eluted from Hep-PLL-Sepharose by 0.5 M NaCl than that from Hep-Sepharose, as shown by antibody reactivity, while the specific binding of HMG1 to Hep-Sepharose was confirmed by N-terminal sequencing (data not shown). The results indicate that the CypA of both rat and pig binds to the pseudoPG adsorbents. A heparin-binding site of CypA is highly conserved among human, pig, and rat in a short amino acid sequence, '*R*NG*K*TS*KK*' (4 essential amino acids are underlined), that is present at the C-terminal region [12]. If this region is responsible for the binding of CypA to the BPL-Hep probe, multimerization of CypA may be necessary for recognition of the macromolecular structure of pseudoPG. Thus, SDS-PAGE was carried out under a nonreducing condition to deduce how CypA recognized the

t1.1 **Table 1** Kinetic parameters for the interaction of lactoferrin, thrombin and AT III with immobilized BPL-Hep or biotin hydrazide-Hep

t1.2		BPL-Hep probe			Biotin hydrazide-Hep probe		
t1.3		k_a (s)	k_d (s^{-1})	K_d (M)	k_a (s)	k_d (s^{-1})	K_d (M)
t1.4	Lactoferrin	1.9×10^{6}	2.3×10^{-3}	1.2×10^{-9}	1.5×10^{6}	6.4×10^{-2}	4.4×10^{-8}
t1.5	Thrombin	3.1×10^{3}	2.0×10^{-3}	6.6×10^{-7}	9.5×10^{2}	1.7×10^{-3}	1.8×10^{-6}
t1.6	AT	54	1.5×10^{-4}	2.8×10^{-6}	–	–	–

t1.7 BPL-Hep- and biotin hydrazide-Hep-immobilized sensor chips were prepared as described in the text. Immobilized amounts were 350 RU for BPL-Hep, and 285 RU for biotin hydrazide-Hep. The k_a, k_d, and K_d values were calculated by global fitting using BIAevaluation 3.1 software

higher-order structure of pseudoPG. As shown in Fig. 5d, CypA in the porcine brain extract was found at the upper edge of the separation gel, indicating that CypA was multimerized or complexed with other protein(s) to become a high-molecular weight complex that is stabilized by disulfide bridges in the brain extract.

Discussion

In this study, we synthesized pseudoPGs for the first time. There have been many conjugation studies by several groups, in which polysaccharides were coupled with synthetic polymers. However, most conjugates in those studies were synthesized using nonpolypeptide backbone materials as backbone molecules; such as polyethylene,

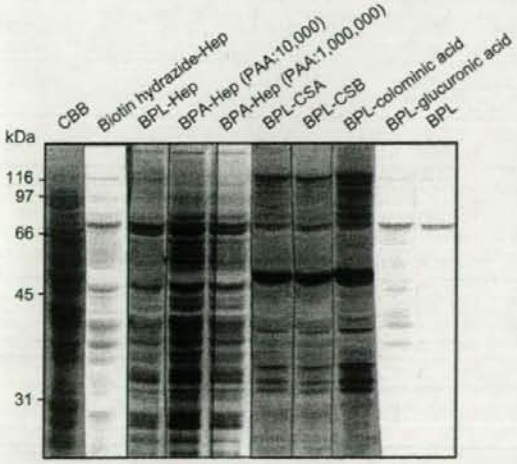

Fig 3 Reactivity of biotin hydrazide Hep, BPL-GAGs, and BPA-Hep probes with rat brain extracts. Extracts (8 μg) were subjected to SDS-PAGE on 9.5% polyacrylamide gels, and Western blotting was performed on PVDF membranes. Proteins were stained with CBB or allowed to react with biotin hydrazide-Hep, BPL-GAGs, and BPA-Hep probes, as described in the text. Molecular mass markers are shown on the left-hand side

[13, 14] and a hydrophobic 1-octanethiol-coated sensorchip surface [15]. Even in the studies where poly L-lysine was used as a backbone, neutral oligosaccharides or unsulfated polysaccharide such as fucose, lactose, dextran, or hyaluronic acid were used as glycan moieties [16, 17]. The conjugates have a clustered carbohydrate determinant; however, the glycan chains, which are important to characterize the ligand-binding activity of proteoglycans, are quite different from those of natural PG monomers. On this context, the pseudoPG is the first to simulate a natural proteoglycan structure having a linear neutral polypeptide backbone and sulfated GAGs.

Glycosylated PLLs have been conventionally developed to target oligonucleotides and genes as nonviral carriers using oligosaccharides [16], dextran, and hyaluronic acid [17, 18]. The greatest difference between the pseudoPGs and the gene carriers is that the gene carriers retain free amino groups of PLL to interact with DNA, while the amino groups in the pseudoPGs were blocked after coupling with GAG by biotinylation and subsequent N-acetylation to suppress electrostatic interaction of the core polymer. Heparin rather than heparan sulfate was mostly used to detect the PG-binding proteins in this study because of its high reactivity with the heparin/heparan sulfate-binding proteins. The heparin-pseudoPG best simulates a natural heparin-clustered proteoglycan such as the serglycin of the secretory vesicles in mast cells [19], and it also simulates heparan sulfate proteoglycan such as syndecan [20].

The binding characteristics of pseudoPG probes were evaluated by SPR, membrane analysis, and affinity chromatography, taking appropriate controls for each assay. A pseudoPG probe, BPL-Hep, exhibited higher affinity toward the known heparin-binding plasma proteins on SPR than the single-strand probe biotin-hydrazide-Hep (Fig. 2 and Table 1). The increased affinity of BPL-Hep over biotin-hydrazide-Hep would be attributable to the multivalent, myriapod-like structure of the proteoglycan. The applicability of pseudoPG probes containing different GAGs to the sensitive detection on a membrane was shown for the binding proteins even after denaturation by SDS and electroblotting. PseudoPG adsorbents showed remarkable

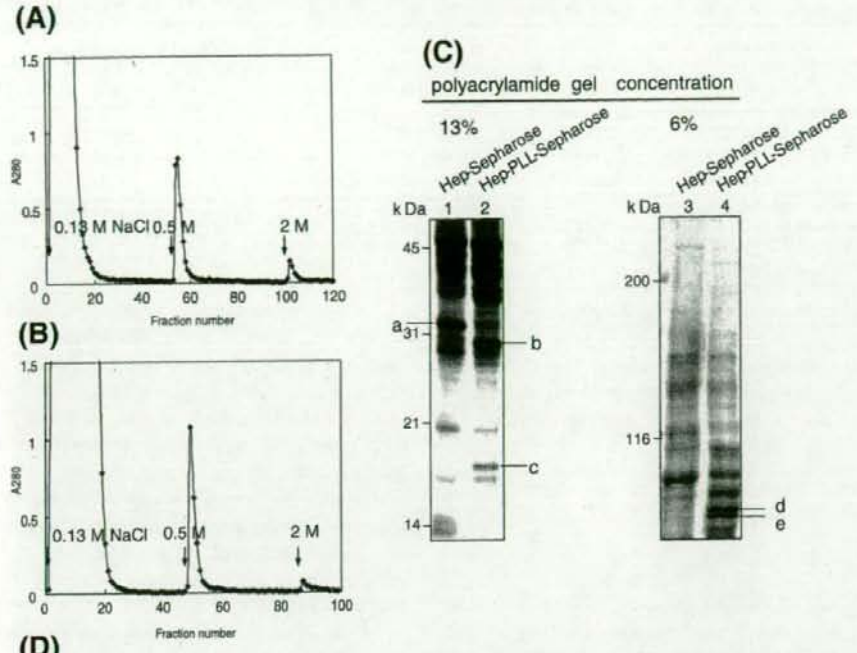

(D)

Band No.	MW (kDa)	N-terminal sequence	Identified protein	Bound & eluted from
a	32	GKGDPKKPRG	amphoterin (HMG1)	Hep-Sepharose
b	30	blocked N-terminal	-	Hep-PLL-Sepharose
c	18	VNPTVFFDIT	cyclophilin A (CypA)	Hep-PLL-Sepharose
d	95	PEETQTQD	HSP90-α	Hep-PLL-Sepharose
e	94	PEEV	HSP90-β	Hep-PLL-Sepharose

Fig 4 Affinity chromatography of rat brain extract on Hep-Sepharose (**a**) or Hep-PLL-Sepharose (**b**) column. Identification of the bound proteins by SDS-PAGE (**c**) and N-terminal amino acid sequences (**d**). **a** Eight milliliters of rat brain extract was incubated with 8 ml of acetoamido-Sepharose for 3 h at 4°C with shaking and packed into a column (2×2.6 cm). The flow-through fractions were collected, incubated with 2 ml of Hep-Sepharose overnight at 4°C with shaking, and packed into a column (0.75×4.5 cm). After washing the column with 0.13 M PBS, the bound materials were eluted with 0.5 M PBS and subsequently with 2 M PBS at the points indicated by *arrows*. Elution was monitored at 280 nm for protein. **b** Ten milliliters of rat brain extract was incubated with 10 ml of PLL-Sepharose. The subsequent procedure was the same as described in (**a**) except incubation with 2 ml of Hep-PLL-Sepharose instead of Hep-Sepharose as the second affinity adsorbent. (**c**) SDS-polyacrylamide gel electrophoresis of 0.5 M NaCl-eluted fractions from a Hep-Sepharose or Hep-PLL-Sepharose column. Each fraction (8 μg protein/lane) was subjected to SDS-PAGE on 13% (**a**) or 6% (**b**) polyacrylamide gels under the reducing condition and transferred to a PVDF membrane. Proteins were stained with CBB. *Lanes 1 and 3* fractions eluted from Hep-Sepharose, *lanes 3 and 4* fractions eluted from Hep-PLL-Sepharose. **d** Direct N-terminal sequencing of each protein in (**c**) was performed on the excised PVDF membrane using a protein sequencer, and proteins were identified by searching the N-terminal 4-10 amino acid sequences in the SWISSPROT database

binding specificity toward several heparin-binding proteins in the rat brain extract (Figs. 3 and 4). The proteins that specifically bound to Hep-PLL-Sepharose were CypA and HSP90α and -β. The pseudoPG probes prepared here proved useful in detection and separation of the PG-binding substances, and they will be applied in finding recognition events that involve higher-order PG structures.

HSP90 is a major molecular chaperone involved in the folding and activation of substrate proteins [21]; it presents two isoforms, HSP 90α and HSP 90β, the functional differences of which have not been clarified yet [22]. HSP90 has two heparin-binding sites [23] that may be responsible for the binding with Hep-PLL. On the one hand, HSP90 forms a complex with client proteins to

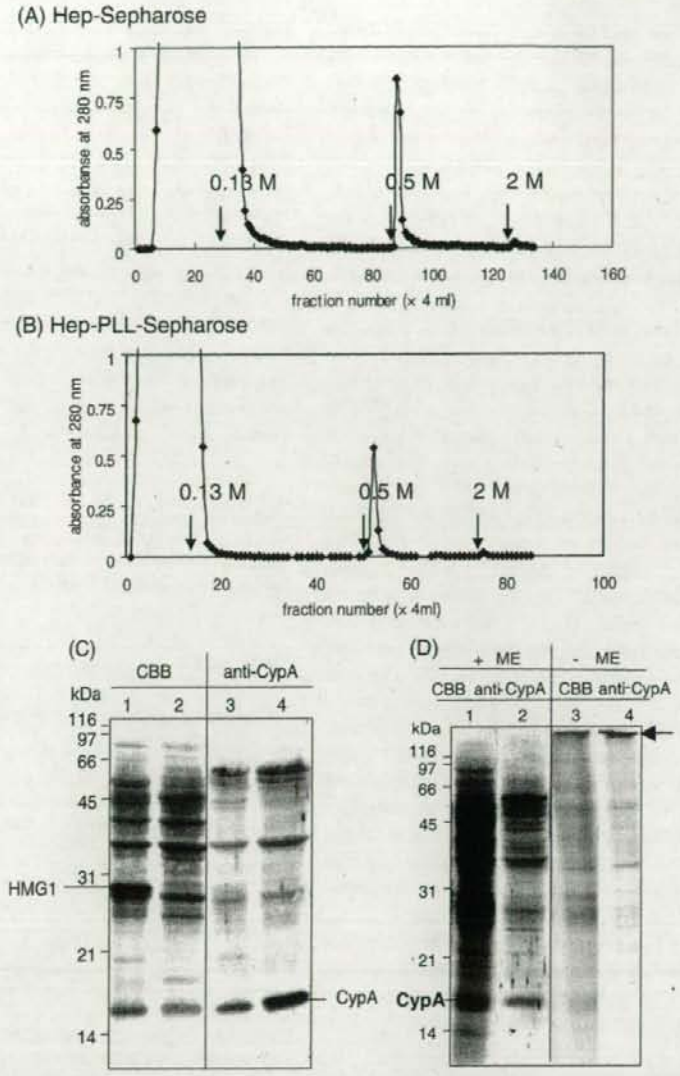

Fig 5 Affinity chromatography of pig brain extract on a Hep-Sepharose column (**a**) or Hep-PLL-Sepharose column (**b**). SDS-PAGE of 0.5 M NaCl-eluted fractions (**c**, **d**). **a** Extracts from pig brain (90 ml, 2.92 mg/ml protein) were applied to an *N*-acetyl Sepharose precolumn (Vt=6 ml, 1.5×3.5 cm). The flow-through fractions were collected and applied to a Hep-Sepharose column (Vt=4 ml, 1.5×2.5 cm). After washing the column with 0.13 M NaCl–PB (first arrow), the bound proteins were eluted with 0.5 and 2 M NaCl-PB at points indicated by *arrows*. Elution was monitored at 280 nm for protein. **b** Extracts from pig brain were applied to a PLL-Sepharose precolumn (Vt=6 ml, 1.5×3.5 cm). The flow-through fractions were collected and applied to a Hep-PLL-Sepharose column (Vt=3 ml, 1.5×2 cm). Elution and protein monitoring were performed in the same way as in A. **c** Fractions eluted from Hep-Sepharose or Hep-PLL-Sepharose (10 μg protein/lane) were subjected to SDS-PAGE on 15% polyacrylamide gels under the reducing condition, and Western blotting on a PVDF membrane was performed. Proteins were stained with CBB (*lanes 1, 2*) or reacted with anti-CypA (*lanes 3, 4*). *Lanes 1, 3* Fractions eluted 0.5 M NaCl from a Hep-Sepharose column. *Lanes 2, 4* Fractions eluted by 0.5 M NaCl from a Hep-PLL-Sepharose column. Molecular weight markers are shown on the *left*. **d** The fraction eluted by 0.5 M NaCl from a Hep-PLL-Sepharose column was electrophoresed under reducing (*lanes 1, 2*) or non-reducing condition (*lanes 3, 4*) and transferred onto a PVDF membrane. Proteins were stained with CBB (*lanes 1, 3*) or reacted with anti-CypA and developed with DAB/H_2O_2 (*lanes 2, 4*). Molecular weight markers are shown on the *left*

stabilize them. On the other hand, CypA was recently found in a heterocomplex of potential sorting proteins containing HSP90 and other chaperonins to traffic asialoglycoprotein receptors between the plasma membrane and the endosomal pool [24]. The high-molecular-weight band observed on SDS-PAGE under the nonreducing condition (Fig. 5d) might be such a heterocomplex that includes CypA. Furthermore, CypA and Hsp90s are secreted into the extracellular space by the above mentioned vesicular traffic pathways [25, 26], which allows them to encounter heparan sulfate proteoglycans.

CypA is a peptidyl-prolyl isomerase that binds the immunosuppressive drug cyclosporin A to modulate T cell differentiation and proliferation. It is widely expressed in multiple tissues, especially abundantly in the brain [27]. In this study, CypA was found to bind pseudoPG Sepharose in spite of its small heparin-binding site by forming multimers or complexes with other protein(s) to become a high-molecular-weight complex (Fig. 5d). CypA has been reported to be involved in an initial process of HIV-1 attachment to macrophages by interacting with a heparan sulfate PG, syndecan, which serves as an attachment receptor at the cell surface [12, 28]. In addition, CypA was shown to contribute to the subsequent infection process by modulating the response of HIV-1to host restriction factors [29]. Interestingly, it has been reported that Hsp60 and HSP70 family proteins are incorporated into HIV-1 and -2 similar to the incorporation of CypA into HIV-1. In this context, this study proposes that a PG structure of cell surface heparan sulfate is important for recognition of CypA and HSP family proteins at the initial attachment of HIV-1. In that case, pseudoPG may serve as a potent inhibitor or investigation probe for syndecan-HIV-1 interaction.

A few problems still remain for the efficient synthesis of pseudoPGs; one question is the possibility that an unsubstituted amino group in the glucosamine present in the heparin chain might react during biotinylation of Hep-PLL with NHS-biotin, or immobilization of Hep-PLL to formyl Sepharose. However, the concentration of free amino groups in heparin is small and has been reported by Osmond *et al.* to be 1/10 (mol/mol heparin) [30]. Under the reaction condition in this study, the amino groups in PLL are present in about 10^4-fold excess of that of free amino groups in heparin. Therefore, the possibility of interference by heparin underivatized with PLL would be negligible even if N-unsubstituted glucosamine is present and biotinylated before injection onto the sensor chip, or if it reacts to formyl Sepharose during the preparation of affinity adsorbent.

The low yield of reductive amination for sulfated GAGs is a challenge that remains to be solved. Although the RI signal indicated that the generation of pseudoPGs is minute (Fig. 1), the binding specificities of pseudoPGs and the biotin-hydrazide-heparin probe are distinct from each other (Table 1, Figs. 3, 4, and 5) and the reactivity is different among the pseudoPG probes, depending on the glycan chains (Fig. 3). The introduction of a biotin group into the pseudoPG probe allows concentration of the probe on the SA-sensor chip and detection of the binding proteins on the membrane at high sensitivity. Suda *et al.* reported that reductive amination of sulfated GAG proceeds almost quantitatively with aromatic amines at pH 3–4, and this may improve the yield of pseudoPGs [15, 31]. Using polymers of an aromatic amine instead of PLL as the backbone may also enhance the production of pseudoPGs. To improve the efficiency of the pseudoPG probes, preparations using various skeletal polymers are under examination in our laboratory.

Acknowledgements This work was supported in part by Grants-in-aid for Scientific Research on Priority Areas 15040209 and 17046004 (HO) from the Ministry of Education, Culture, Sports, Science, and Technology and by a Research Grant on HIV/AIDS from the Ministry of Health Labour Sciences Research. We thank K. Ono for editing the English.

References

1. Iozzo, R.V.: Annu. Rev. Biochem. **67**, 609–652 (1998). doi:10.1146/annurev.biochem.67.1.609
2. Bernfield, M., Gotte, M., Park, P.W., Reizes, O., Fitzgerald, M.L., Lincecum, J., Zako, M.: Annu. Rev. Biochem. **68**, 729–777 (1999). doi:10.1146/annurev.biochem.68.1.729
3. Langford, J.K., Stanley, M.J., Cao, D., Sanderson, R.D.: J. Biol. Chem. **273**(45), 29965–29971 (1998). doi:10.1074/jbc.273.45.29965
4. Sugahara, K., Mikami, T.: Curr. Struct. Opin. Biol. **17**(5), 536–545 (2007). doi:10.1016/j.sbi.2007.08.015
5. Schwartz, N.B., Domowicz, M.: Glycoconj. J. **21**(6), 329–341 (2004). doi:10.1023/B:GLYC.0000046278.34016.36
6. Seno, N., Anno, K., Kondo, K., Nagase, S., Saito, S.: Anal. Biochem. **37**(1), 197–202 (1970). doi:10.1016/0003-2697(70)90280-0
7. Ogawa, H., Ueda, H., Natsume, A., Suzuki, R.: Methods Enzymol **362**, 196–209 (2003). doi:10.1016/S0076-6879(03)01013-9
8. Ito, Y., Seno, N., Matsumoto, I.: J. Biochem. **97**(6), 1689–1694 (1985)
9. Sasaki, H., Hayashi, A., Kitagaki-Ogawa, H., Matsumoto, I., Seno, N.: J. Chromatogr. A **400**, 123–132 (1987). doi:10.1016/S0021-9673(01)81605-8
10. Matsumoto, I., Kitagaki, H., Akai, Y., Ito, Y., Seno, N.: Anal. Biochem. **116**(1), 103–110 (1981). doi:10.1016/0003-2697(81)90329-8
11. Laemmli, U.K.: Nature **227**(5259), 680–685 (1970). doi:10.1038/227680a0
12. Saphire, A.C., Bobardt, M.D., Gallay, P.A.: EMBO J **18**(23), 6771–6785 (1999). doi:10.1093/emboj/18.23.6771
13. Paulsson, M., Gouda, I., Larm, O., Ljungh, A.: J. Biomed. Mater. Res. **28**(3), 311–317 (1994). doi:10.1002/jbm.820280305
14. Klein, J., Kraus, M., Ticha, M., Zelezna, B., Jonakova, V., Kocourek, J.: Glycoconj. J. **12**(1), 51–54 (1995). doi:10.1007/BF00731868

15. Suda, Y., Arano, A., Fukui, Y., Koshida, S., Wakao, M., Nishimura, T., Kusumoto, S., Sobel, M.: Bioconjug. Chem. **17** (5), 1125–1135 (2006). doi:10.1021/bc0600620
16. Stewart, A.J., Pichon, C., Meunier, L., Midoux, P., Monsigny, M., Roche, A.C.: Mol. Pharm. **50**(6), 1487–1494 (1996)
17. Asayama, S., Nogawa, M., Takei, Y., Akaike, T., Maruyama, A.: Bioconjug. Chem. **9**(4), 476–481 (1998). doi:10.1021/bc970213m
18. Asayama, S., Maruyama, A., Akaike, T.: Bioconjug. Chem. **10**(2), 246–253 (1999). doi:10.1021/bc980093y
19. Kresse, H., Hausser, H., Schonherr, E.: Experientia **49**(5), 403–416 (1993). doi:10.1007/BF01923585
20. Tumova, S., Woods, A., Couchman, J.R.: Int. J. Biochem. Cell Biol. **32**(3), 269–288 (2000). doi:10.1016/S1357-2725(99)00116-8
21. Yahara, I., Minami, Y., Miyata, Y.: Ann. N. Y. Acad. Sci. **851**, 54–60 (1998). doi:10.1111/j.1749-6632.1998.tb08976.x
22. Minami, Y., Kawasaki, H., Miyata, Y., Suzuki, K., Yahara, I.: J. Biol. Chem. **266**(16), 10099–10103 (1991)
23. Itoh, H., Tashima, Y.: Int. J. Biochem. **25**(2), 157–161 (1993). doi:10.1016/0020-711X(93)90003-W
24. Huang, T., Deng, H., Wolkoff, A.W., Stockert, R.J.: J. Biol. Chem. **277**(40), 37798–37803 (2002). doi:10.1074/jbc.M204786200
25. Suzuki, J., Jin, Z.G., Meoli, D.F., Matoba, T., Berk, B.C.: Circ. Res. **98**(6), 811–817 (2006). doi:10.1161/01.RES.0000216405.85080.a6
26. Li, W., Li, Y., Guan, S., Fan, J., Cheng, C.F., Bright, A.M., Chinn, C., Chen, M., Woodley, D.T.: EMBO J. **26**(5), 1221–1233 (2007). doi:10.1038/sj.emboj.7601579
27. Goldner, F.M., Patrick, J.W.: J. Comp. Neurol. **372**(2), 283–293 (1996). doi:10.1002/(SICI)1096-9861(19960819)372:2<283::AID-CNE9>3.0.CO;2-#
28. Saphire, A.C., Bobardt, M.D., Zhang, Z., David, G., Gallay, P.A.: J. Virol. **75**(19), 9187–9200 (2001). doi:10.1128/JVI.75.19.9187-9200.2001
29. Towers, G.J., Hatziioannou, T., Cowan, S., Goff, S.P., Luban, J., Bieniasz, P.D.: Nat. Med. **9**(9), 1138–1143 (2003). doi:10.1038/nm910
30. Osmond, R.I., Kett, W.C., Skett, S.E., Coombe, D.R.: Anal. Biochem. **310**(2), 199–207 (2002). doi:10.1016/S0003-2697(02)00396-2
31. Koshida, S., Suda, Y., Arano, A., Sobel, M., Kusumoto, S.: Tetrahedron Lett **42**(7), 1293 (2001). doi:10.1016/S0040-4039(00)02277-2

AUTHOR QUERY

AUTHOR PLEASE ANSWER QUERY.

Q1. Subpanel labels were inserted in the caption. Please check if appropriate.

TRAF6 distinctively mediates MyD88- and IRAK-1-induced activation of NF-κB

Masashi Muroi and Ken-ichi Tanamoto[1]

Division of Microbiology, National Institute of Health Sciences, Tokyo, Japan

Abstract: MyD88 and IL-1R-associated kinase 1 (IRAK-1) play crucial roles as adaptor molecules in signal transduction of the TLR/IL-1R superfamily, and it is known that expression of these proteins leads to the activation of NF-κB in a TNFR-associated factor 6 (TRAF6)-dependent manner. We found in this study, however, that a dominant-negative mutant of TRAF6, lacking the N-terminal RING and zinc-finger domain, did not inhibit IRAK-1-induced activation of NF-κB in human embryonic kidney 293 cells, although the TRAF6 mutant strongly suppressed the MyD88-induced activation. The dominant-negative mutant of TRAF6 did not affect the IRAK-1-induced activation, regardless of the expression level of IRAK-1. In contrast, small interfering RNA silencing of TRAF6 expression inhibited MyD88-induced and IRAK-1-induced activation, and supplementation with the TRAF6 dominant-negative mutant did not restore the IRAK-1-induced activation. Expression of IRAK-1, but not MyD88, induced the oligomerization of TRAF6, and IRAK-1 and the TRAF6 dominant-negative mutant were associated with TRAF6. These results indicate that TRAF6 is involved but with different mechanisms in MyD88-induced and IRAK-induced activation of NF-κB and suggest that TRAF6 uses a distinctive mechanism to activate NF-κB depending on signals. *J. Leukoc. Biol.* 83: 702–707; 2008.

Key Words: *Toll-like receptor · IL-1 receptor · lipopolysaccharide*

INTRODUCTION

TLR/IL-1R family members share common intracellular signaling proteins including MyD88, the IL-1R-associated kinase (IRAK) family, and TNFR-associated factor 6 (TRAF6) [1, 2]. Ligand binding triggers the recruitment of MyD88 to the Toll/IL-1R (TIR) domain of TLR/IL-1R via a homophilic TIR–TIR interaction, which in turn, recruits IRAK-4 and IRAK-1 into the receptor complex. IRAK-4 does not bind IRAK-1 directly but is recruited into the complex through binding with MyD88. This allows IRAK-1 and IRAK-4 to come in close proximity, which induces IRAK-4 to phosphorylate IRAK-1 [3], probably triggering autophosphorylation of IRAK-1. Autophosphorylated IRAK-1 interacts with TRAF6 [4], leading to the activation of NF-κB [1].

MyD88 is known as a universal adaptor molecule that interacts with IL-1R and most of TLRs. MyD88 consists of an N-terminal death domain separated by a short internal linker from a C-terminal TIR domain, which is necessary for the interaction with the TIR domain of TLR/IL-1R. The death domain and the internal linker domain have been implicated in the interaction with IRAK-1 and IRAK-4, respectively [5]. IRAK-1 consists of an N-terminal death domain, which is involved in the binding of MyD88 [6], and a central serine/threonine kinase domain. The C-terminal region of IRAK-1 contains three potential TRAF6-binding sites, and mutation of the amino acids (Glu^{544}, Glu^{587}, Glu^{708}) in these sites to alanine greatly reduces activation of NF-κB [7]. The death domain and the internal domain between the death domain and the kinase domain of IRAK-1 are also involved in binding TRAF6. The N-terminal region (death domain and internal domain) and the first half of the C-terminal region are sufficient for IL-1-induced activation of NF-κB [8].

It is known that all of MyD88, IRAK-1, and TRAF6 are involved in TLR/IL-R signaling to activate NF-κB. However, it is still enigmatic how these molecules lead to the activation of NF-κB [9]. Polyubiquitination of TRAF6 is reportedly important for TLR/IL-1R signaling [10]. TRAF6 itself functions, in conjunction with the ubiquitin-conjugating enzyme complex Ubc13-Uev1A, as a ubiquitin ligase that catalyzes the formation of unique Lys^{63}-linked polyubiquitin chains [11, 12]. TRAF6 catalyzes Lys^{63}-linked polyubiquitination on TRAF6 itself, and the polyubiquitinated TRAF6 activates NF-κB signaling proteins by a proteasome-independent mechanism [11, 12]. On the other hand, it has also been reported that oligomerization of TRAF6 induces activation of NF-κB [12, 13]. However, the relationship between the polyubiquitination and the oligomerization is unknown, and the role of MyD88 and IRAK-1 in these events is still ambiguous. We report here for the first time in our knowledge that TRAF6 distinctively mediates MyD88-induced and IRAK-1-induced activation of NF-κB and that only IRAK-1 leads to oligomerization of TRAF6.

[1] Correspondence: Division of Microbiology, National Institute of Health Sciences, 1-18-1 Kamiyoga, Setagaya, Tokyo 158-8501, Japan. E-mail: tanamoto@nihs.go.jp

Received September 13, 2007; revised November 9, 2007; accepted November 12, 2007.

doi: 10.1189/jlb.0907629

0741-5400/08/0083-702

MATERIALS AND METHODS

Cell culture and reagents

The human embryonic kidney (HEK)293 cell line (obtained from the Human Science Research Resources Bank, Tokyo, Japan) was grown in DMEM (Invitrogen, Carlsbad, CA, USA), supplemented with 10% (v/v) heat-inactivated FCS (Invitrogen), penicillin (100 U/ml), and streptomycin (100 μg/ml). *Escherichi coli* O111:B4 LPS was obtained from Sigma-Aldrich (St. Louis, MO, USA) and was repurified according to the method described by Hirschfeld et al. [14]. A stable cell population expressing FLAG-tagged TRAF6 and equine infectious anaemia virus epitope (EIAV)-tagged TRAF6 was established as follows. After linearizing with *Bgl*II, expression plasmids encoding FLAG-tagged TRAF6 and EIAV-tagged TRAF6 were transfected into HEK293 cells by the calcium phosphate precipitation method. Transfected cells were selected for G418 resistance at a concentration of 1 mg/ml. An antiserum against the EIAV-tag epitope (amino acid sequence: ADRRIPCTAEE) was a kind gift from Dr. Nancy Rice (National Cancer Institute-Frederick Cancer Research and Development Center, Frederick, MD, USA). Antibodies against TRAF6 (H-274, Santa Cruz Biotechnology, Santa Cruz, CA, USA) and FLAG-epitope (M2, Sigma-Aldrich) were used. Anti-FLAG M2 affinity gel was from Sigma-Aldrich. A *TRAF6 small interfering* (si)RNA oligo (CCACGAAGAG-AUAAUGGAUdTdT) [15] was synthesized by Qiagen (Valencia, CA, USA).

Plasmids

The coding regions of human MyD88 and IκB kinase β (IKKβ) were amplified by RT-PCR from total RNA prepared from human spleen (OriGene Technologies, Rockville, MD, USA) and THP-1 cells, respectively. The coding region of human TRAF6 was amplified from a human spleen cDNA library (Clontech, Palo Alto, CA, USA). A plasmid containing human IRAK-1 cDNA was obtained from the Mammalian Gene Collection (http://mgc.nci.nih.gov/). Deletions found in the IRAK-1 plasmid were corrected by PCR-mediated mutagenesis. The coding regions of all of these constructs were subcloned into mammalian expression vectors containing the N-terminal EIAV-tag and FLAG-tag epitope sequences. NF-κB-dependent luciferase reporter plasmid pELAM-1, was described previously [16]. All mutant plasmids were created by PCR-mediated mutagenesis, and mutations were confirmed by DNA sequencing.

NF-κB reporter assay, RNA interference, immunoprecipitation, and immunoblotting

The NF-κB-dependent luciferase reporter assay was performed as described elsewhere [17]. Briefly, HEK293 cells ($2–5\times10^5$ cells) were plated in six-well plates and transfected the following day by the calcium phosphate precipitation method with the indicated plasmids plus 0.2 μg pELAM-1, and 5 ng phRL-TK (Promega, Madison, WI, USA) for normalization. At 24–32 h after transfection, cellular extracts were prepared by adding a lysis buffer [10 mM HEPES-KOH, pH 7.9, 10 mM KCl, 5 mM EDTA, 40 mM β-glycerophosphate, 0.5% Nonidet P-40 (NP-40), 30 mM NaF, 1 mM Na_3VO_4, 100 nM okadaic acid] containing a protease inhibitor cocktail (Roche Diagnostics, Mannheim, Germany). Reporter gene activity was measured with a portion of the cellular extract, according to the manufacturer's (Promega) instruction. To another portion of the cellular extract, anti-FLAG M2-agarose (Sigma-Aldrich) was added, and the mixture was incubated at 4°C for 1 h. The agarose was washed three times with PBS containing 0.5% NP-40, and bound proteins were subsequently eluted from the agarose by incubating with 1% SDS. The resulting supernatant was subjected to SDS-PAGE. Proteins were transferred to a polyvinylidene difluoride membrane (Immobilon-P, Millipore, Bedford, MA, USA) and subjected to immunoblotting with the indicated antibodies. The signals were visualized by using an enhanced chemiluminescence system (GE Healthcare Bio-sciences, Piscataway, NJ, USA). For RNA interference, HEK293 cells ($1–3\times10^5$ cells) were plated in six-well plates and transfected the following day by the calcium phosphate precipitation method with the indicated amounts of a siRNA oligo. On the following day after the first transfection, reporter plasmids, indicated expression plasmids, and the siRNA oligo were transfected further as described above. The transfected amount of siRNA oligo was normalized by supplementing an unrelated oligo. At 24–32 h after the second transfection, cellular extracts were prepared, and reporter activities were determined as above.

RESULTS

A dominant-negative *mutant* of TRAF6 inhibits MyD88-induced but not IRAK-1-induced activation of NF-κB

To explore the involvement of TRAF6 in MyD88- and IRAK-1-induced activation of NF-κB, we examined the effects of a dominant-negative mutant of TRAF6. It is well known that the deletion of the N-terminal RING and zinc-finger domain (aa 1–288) of TRAF6 abolishes the ability of TRAF6 to mediate IL-1- and LPS-induced activation of NF-κB [18] and that the N-terminal deletion mutant acts as a dominant-negative mutant [4]. Thus, this N-terminal deletion mutant of TRAF6 was expressed with MyD88 or IRAK-1 and measured NF-κB-dependent reporter activity in HEK293 cells (**Fig. 1**). As expected, the expression of MyD88 activated NF-κB, and the coexpression of the TRAF6 deletion mutant inhibited this activation in a dose-dependent manner. However, IRAK-1-induced activation of NF-κB was surprisingly unaffected by coexpression of the deletion mutant. On the other hand, MyD88- and IRAK-1-induced activation of NF-κB were inhibited by a kinase-dead mutant (K44A) of IKKβ, indicating that the activation induced by MyD88 and IRAK-1 is IKK-dependent. The expression levels of MyD88 and IRAK-1 were not affected by coexpression of the TRAF6 deletion mutant (Fig. 1, lower panels).

To confirm the inability of the TRAF6 deletion mutant to inhibit IRAK-1-induced activation of NF-κB, the effect of the deletion mutant was examined further by changing the expression levels of MyD88 and IRAK-1 (**Fig. 2**). The TRAF6 deletion mutant inhibited MyD88-induced activation of NF-κB (Fig. 2A, right), irrespective of the MyD88 expression level (Fig. 2B); however, IRAK-1-induced activation was not af-

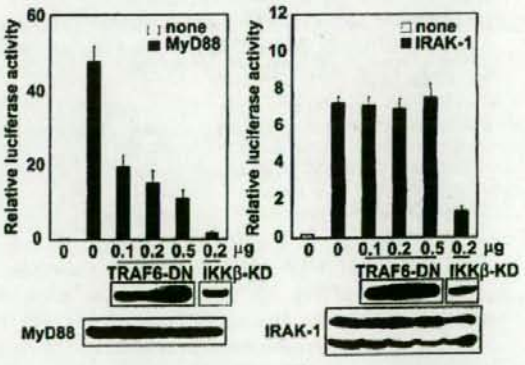

Fig. 1. A TRAF6 dominant-negative mutant inhibits MyD88-induced but not IRAK-1-induced activation of NF-κB. HEK293 cells were transiently transfected with a NF-κB-dependent luciferase reporter plasmid and an expression plasmid (0.1 μg) for MyD88 (left panel) or IRAK-1 (right panel) together with a kinase-dead (KD) mutant of IKKβ (K44A) or an increasing amount of a dominant-negative mutant plasmid for TRAF6 (TRAF6-DN; aa 289–522). After 30 h, cellular extracts were subjected to luciferase activity measurements and SDS-PAGE followed by immunoblotting. Values are means ± SEM from three independent experiments.

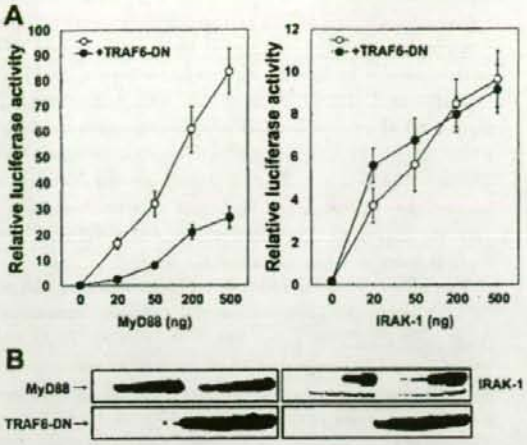

Fig. 2. A TRAF6 dominant-negative mutant did not affect IRAK-1-induced activation at any of the IRAK-1 expression levels. HEK293 cells were transiently transfected with a NF-κB-dependent luciferase reporter plasmid and an increasing amount of MyD88 (A) or IRAK-1 (B) expression plasmid in the absence (○) or presence (●) of a dominant-negative mutant plasmid (0.5 μg) for TRAF6 (TRAF6-DN; aa 289–522). After 30 h, cellular extracts were subjected to luciferase activity measurements and SDS-PAGE followed by immunoblotting. Values are means ± SEM from three independent experiments.

fected (Fig. 2A, left) at any of the IRAK-1 expression levels (Fig. 2B).

MyD88-induced and IRAK-1-induced activation of NF-κB require TRAF6

Results obtained with the TRAF6 dominant-negative suggest that TRAF6 is not involved in IRAK-1-induced activation of NF-κB. To confirm this finding, the effects of a TRAF6 siRNA were examined. An increasing amount of a TRAF6 siRNA oligo was transfected into HEK293 cells with MyD88, IRAK-1, or IKKβ, and NF-κB-dependent reporter activity was measured. Unexpectedly, IRAK-1-induced (**Fig. 3B**) as well as MyD88-induced (Fig. 3A) activation of NF-κB was inhibited by the transfection of the siRNA oligo in a dose-dependent manner. IKKβ-induced activation of NF-κB was not significantly affected by the siRNA oligo (Fig. 3C), indicating that the inhibition was not nonspecific. The expression levels of MyD88, IRAK-1, and IKKβ were not affected by the TRAF6 siRNA oligo (Fig. 3, upper panels). Furthermore, another TRAF6 siRNA oligo that targets different regions of TRAF6 mRNA also inhibited MyD88 and IRAK-1-induced activation of NF-κB (data not shown). These results indicate that although IRAK-1-induced activation was not inhibited by a TRAF6 dominant-negative mutant, MyD88- and IRAK-1-induced activation of NF-κB require TRAF6.

The N-terminal region of TRAF6 is believed to be important for signal transduction. However, as IRAK-1-induced activation of NF-κB was not affected by an N-terminal deletion mutant of TRAF6 but required TRAF6, the possibility that the C-terminal portion of TRAF6 is involved in IRAK-1-induced activation of NF-κB still remains. Thus, the effect of the TRAF6 N-terminal deletion mutant was evaluated after siRNA

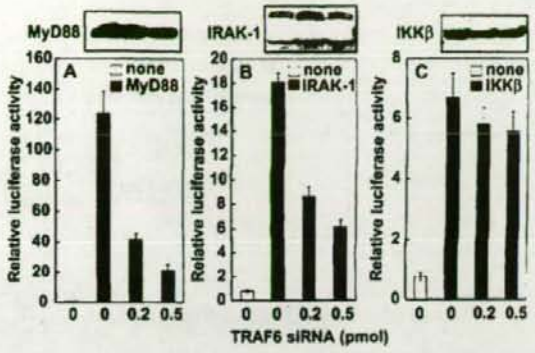

Fig. 3. A TRAF6 siRNA oligo inhibits MyD88-induced and IRAK-1-induced activation of NF-κB. HEK293 cells were transiently transfected with a NF-κB-dependent luciferase reporter plasmid and an expression plasmid (0.1 μg) for MyD88 (A), IRAK-1 (B), or IKKβ (C), together with an increasing amount of a TRAF6 siRNA oligo. After 30 h, cellular extracts were subjected to luciferase activity measurements and SDS-PAGE followed by immunoblotting. Values are means ± SEM from six independent experiments.

silencing of endogenous TRAF6 (**Fig. 4**). The transfection of a TRAF6 siRNA oligo did not affect basal NF-κB-dependent reporter activity. Coexpression of TRAF6, but not expression of the N-terminal deletion mutant, increased reporter activity (Fig. 4, left panel). The significant increase in reporter activity observed upon expression of MyD88 was inhibited by the transfection of the TRAF6 siRNA oligo as shown above. Under this condition, coexpression of TRAF6, but not the TRAF6 N-terminal deletion mutant, overcame the inhibition induced

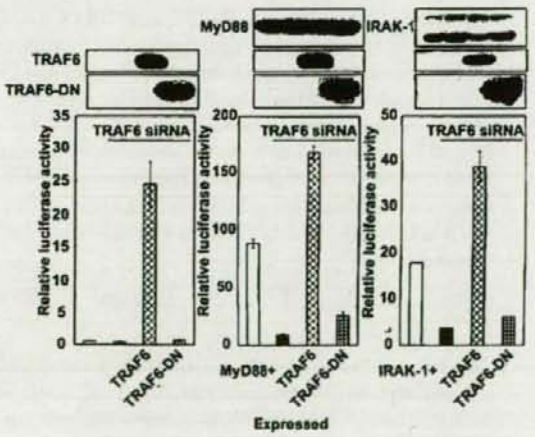

Fig. 4. C-terminal portion of TRAF6 is not involved in IRAK-1-induced activation of NF-κB. HEK293 cells were transiently transfected with a NF-κB-dependent luciferase reporter plasmid and a control vector (left panel), an expression plasmid (0.1 μg) for MyD88 (middle panel), or IRAK-1 (right panel) together with wild-type or a dominant-negative mutant plasmid (0.5 μg) for TRAF6 (TRAF6-DN; aa 289–522) in the absence (left bar) or presence (right three bars) of a TRAF6 siRNA oligo (0.5 pmol). After 30 h, cellular extracts were subjected to luciferase activity measurements and SDS-PAGE followed by immunoblotting. Values are means ± SEM from seven independent experiments.

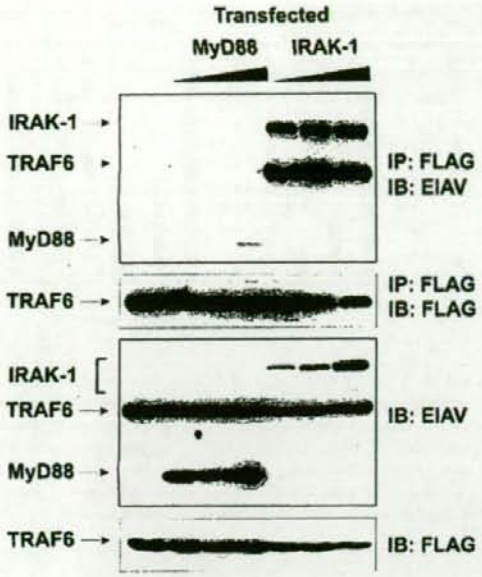

Fig. 5. IRAK-1 but not MyD88 induces oligomerization of TRAF6. HEK293 cells stably expressing FLAG-tagged TRAF6 and EIAV-tagged TRAF6 were transiently transfected with an expression plasmid for EIAV-tagged MyD88 or EIAV-tagged IRAK-1. After 30 h, cellular extracts were prepared, and FLAG-tagged TRAF6 was immunoprecipitated (IP). Precipitated, FLAG-tagged TRAF6 (second panel from top) and coprecipitated EIAV-tagged proteins (top panel) were detected by immunoblotting (IB). Part of each cell extract prepared above was subjected to the detection of EIAV-tagged proteins (second panel from bottom) and FLAG-tagged TRAF6 (bottom panel) by immunoblotting.

by TRAF6 siRNA (Fig. 4, middle panel). IRAK-1-induced activation of NF-κB was also inhibited by TRAF6 siRNA, and coexpression of TRAF6 again overcame the inhibition. However, coexpression of the N-terminal deletion mutant was not able to overcome the inhibition induced by TRAF6 siRNA (Fig. 4, right panel). TRAF6, the N-terminal deletion mutant of TRAF6, IRAK-1, and MyD88, were properly expressed (Fig. 4, upper panels). Thus, it is unlikely that the C-terminal portion of TRAF6 is capable of transmitting IRAK-1-induced activation of NF-κB.

IRAK-1 but not MyD88 induces oligomerization of TRAF6

The effects of the TRAF6 N-terminal deletion mutant differed between MyD88-induced and IRAK-1-induced activation of NF-κB. The fact that TRAF6 is required for both types of activation suggests that TRAF6 is differentially involved in the activation induced by these molecules. As it has been reported that TRAF6 oligomerization induces activation of NF-κB [12, 13], the oligomerization of TRAF6 was examined in response to the expression of MyD88 and IRAK-1. HEK293 cells stably expressing FLAG-tagged TRAF6, and EIAV-tagged TRAF6 were transiently transfected with an expression plasmid for EIAV-tagged MyD88 or EIAV-tagged IRAK-1. After preparing cell extracts, FLAG-tagged TRAF6 was immunoprecipitated (**Fig. 5**, second panel from the top) with anti-FLAG M2 affinity gel, and coprecipitated EIAV-tagged proteins were detected by immunoblotting (Fig. 5, top panel). Upon expression of MyD88, a trace amount of MyD88, but no EIAV-tagged TRAF6, was coprecipitated with FLAG-tagged TRAF6. In contrast, EIAV-tagged TRAF6 as well as IRAK-1 were coprecipitated with FLAG-tagged TRAF6 when IRAK-1 was expressed. MyD88, IRAK-1, EIAV-tagged TRAF6 (Fig. 5, second panel from the bottom), and FLAG-tagged TRAF6 (Fig. 5, bottom panel) were properly expressed. Therefore, expression of IRAK-1 but not MyD88 induces oligomerization of TRAF6.

The effect of the TRAF6 N-terminal deletion mutant on IRAK-1-induced oligomerization of TRAF6 was next examined (**Fig. 6**). HEK293 cells stably expressing FLAG-tagged TRAF6 and EIAV-tagged TRAF6 were transiently transfected with an expression plasmid for EIAV-tagged IRAK-1 and an increasing amount of a plasmid expressing the EIAV-tagged TRAF6 N-terminal deletion mutant. After preparing cell extracts, FLAG-tagged TRAF6 was immunoprecipitated (Fig. 6, right part of the top panel) with anti-FLAG M2 affinity gel, and coprecipitated EIAV-tagged proteins were detected by immunoblotting (Fig. 6, right part of the bottom panel). Upon expression of IRAK-1, EIAV-tagged TRAF6 as well as IRAK-1 were coprecipitated with FLAG-tagged TRAF6 as shown above. When the TRAF6 N-terminal deletion mutant was coexpressed, the mutant was also precipitated with FLAG-tagged TRAF6, and the amount of coprecipitated EIAV-tagged TRAF6 was not affected by coexpression of the TRAF6 N-terminal deletion mutant. IRAK-1, EIAV-tagged and FLAG-tagged TRAF6, and the TRAF6 deletion mutant were expressed properly (Fig. 6, left panels). Thus, the expression of the TRAF6 N-terminal deletion mutant does not appear to inhibit the IRAK-1-induced oligomerization of TRAF6. Taken together, these data demonstrate that TRAF6 is differentially

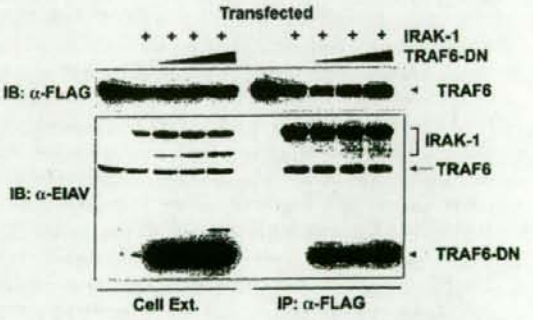

Fig. 6. IRAK-1 and a TRAF6 dominant-negative mutant were coprecipitated with TRAF6. HEK293 cells stably expressing FLAG-tagged TRAF6 and EIAV-tagged TRAF6 were transiently transfected with an increasing amount of a dominant-negative mutant plasmid for EIAV-tagged TRAF6 (TRAF6-DN; aa 289–522) together with an expression plasmid for EIAV-tagged MyD88 or EIAV-tagged IRAK-1. After 30 h, cellular extracts were prepared, and FLAG-tagged TRAF6 was immunoprecipitated. Precipitated FLAG-tagged TRAF6 (right half of top panel) and coprecipitated EIAV-tagged proteins (right half of bottom panel) were detected by immunoblotting. Part of each cell extract (Cell Ext.) prepared above was subjected to the detection of EIAV-tagged proteins (left half of bottom panel) and FLAG-tagged TRAF6 (left half of top panel) by immunoblotting.

involved in MyD88-induced and IRAK-1-induced activation of NF-κB and that IRAK-1 but not MyD88 induces TRAF6 oligomerization.

DISCUSSION

In this study, we found that TRAF6 is differentially involved in MyD88- and IRAK-1-induced activation of NF-κB. MyD88 and IRAK-1 act as adaptor molecules in TLR/IL-1R signaling, and overexpression of each molecule leads to activation of NF-κB via their downstream signaling molecule TRAF6 (see ref. [1]). These observations were confirmed in the experiment in which TRAF6 siRNAs inhibited the activation of MyD88- and IRAK-1-induced NF-κB activation (Fig. 3). However, we found that a dominant-negative mutant of TRAF6 (N-terminal deletion of aa 1–288) inhibits only MyD88-induced activation (Figs. 1 and 2). It is unlikely that IRAK-1 activates NF-κB by using the C-terminal portion of TRAF6, as IRAK-1 failed to activate NF-κB when endogenous, wild-type TRAF6 was silenced by TRAF6 siRNA, and the N-terminal deletion mutant of TRAF6 was overexpressed (Fig. 4). We also found that expression of IRAK-1 but not MyD88 leads to oligomerization of TRAF6 (Fig. 5). It has been reported that oligomerization of TRAF6 induces activation of NF-κB [12, 13]. Thus, oligomerization of TRAF6 is probably involved in the IRAK-1-induced activation of NF-κB. The N-terminal deletion mutant of TRAF6 did not inhibit IRAK-1-induced TRAF6 oligomerization. Instead, the mutant formed a complex with the TRAF6 oligomer (Fig. 6), indicating that the TRAF6 oligomer consists of more than two molecules of TRAF6. This finding explains why the N-terminal deletion mutant of TRAF6 was not able to inhibit IRAK-1-induced activation of NF-κB.

Not only does IRAK-1 induce TRAF6 oligomerization, it is also associated with the TRAF6 oligomer (Fig. 5). We found that an IRAK-1 mutant (E544A/E587A/E706A), in which three putative TRAF6-binding sites were mutated, the mutation known to greatly impair the ability to activate NF-κB [7], did not induce oligomerization of TRAF6 (data not shown), suggesting that TRAF6 molecules form a complex through the binding to IRAK-1. Overexpression of IRAK-1 in HEK293 cells appears mainly as two forms on SDS-PAGE (see Fig. 1), with the slower migrating form recognized as the hyperphosphorylated form of IRAK-1 (see ref. [1]). Interestingly, the slower migrating form of IRAK-1 was predominantly coprecipitated with the TRAF6 oligomer (see Fig. 6). It has been reported that IL-1 stimulation leads to hyperphosphorylation of IRAK-1 by autophosphorylation and to association between phosphorylated IRAK-1 and TRAF6 [1]. Thus, it is likely that autophosphorylated IRAK-1 promotes TRAF6 oligomerization by binding to TRAF6.

Overexpression of MyD88 did not induce detectable TRAF6 oligomerization (Fig. 5), although expression led to a strong activation of NF-κB (Fig. 1). TRAF6 oligomerization in response to TLR/IL-1R stimulation has not been reported. There was also no detectable TRAF6 oligomerization in cells stably expressing FLAG-tagged TRAF6 and HA-tagged TRAF6 in response to IL-1, LPS, or Pam_3CSK_4 stimulation, when these cells were transiently expressed with the IL-1RI/IL-1R accessory protein, CD14/TLR4/myeloid differentiation protein-2 or TLR1/TLR2, respectively, although these stimulations induced a strong activation of NF-κB (data not shown). Thus, it is unlikely that TRAF6 oligomerization is required for the activation of NF-κB in response to TLR/IL-1R stimulation. TRAF6 reportedly functions, in conjunction with ubiquitin-conjugating enzyme complex Ubc13-Uev1A, as a ubiquitin ligase, and this ubiquitin ligase activity is involved in the activation of NF-κB [11, 12]. We found that transfection of a Ubc13 siRNA oligo into HEK293 cells inhibited MyD88-induced activation of NF-κB (data not shown). Therefore, the ubiquitin ligase activity of TRAF6 may be involved in the MyD88-induced activation. Fukushima et al. [19] reported that LPS-induced degradation of IκBα was severely impaired in macrophages and splenocytes isolated from heterozygous $Ubc13^{+/-}$ mice. However, Yamamoto et al. [20] reported that Ubc13-deficient B cells, bone marrow macrophages, and embryonic fibroblasts showed almost normal NF-κB activation in response to LPS, IL-1β, or a bacterial lipoprotein. Thus, further studies are needed to clarify the role of the ubiquitin ligase activity of TRAF6 in TLR/IL-1R signaling.

It is considered that IRAK-1 lies downstream of MyD88 in the TLR/IL-1R signaling processes. Thus, our result that a dominant-negative mutant of TRAF6 inhibited MyD88-induced, but not IRAK-1-induced, activation of NF-κB was surprising. There are two possible explanations for this finding. One is that IRAK-1 is not necessary for TLR/IL-1R signaling. The other is that the activation of NF-κB in response to IRAK-1 overexpression is qualitatively different from the activation induced physiologically in response to TLR/IL-1R stimulation. We are not able to exclude the second possibility. However, it has been reported that macrophages from IRAK-1 knockout mice showed only partial impairment of cytokine production and NF-κB activation in response to TLR4 stimulation [21]. In addition, Kawagoe et al. [22] recently found that the IRAK-1/IRAK-4 double-knockout did not affect macrophage activator lipoprotein peptide-2-induced activation of NF-κB and proposed the existence of a TLR-mediated, IRAK-1/IRAK-4-independent signaling pathway. It is possible that another IRAK member, such as IRAK-2, compensates for the lack of IRAK-1/IRAK-4 in this knockout mouse. However, we also found that IRAK-2-induced activation of NF-κB was not inhibited by a dominant-negative mutant of TRAF6 (data not shown). Therefore, IRAK-1 may not be involved in TLR/IL-1R signaling. This possibility remains to be studied.

ACKNOWLEDGMENTS

This research was supported in part by a grant from the Ministry of the Environment. We thank Yukiko Taguchi for technical assistance.

REFERENCES

1. Janssens, S., Beyaert, R. (2003) Functional diversity and regulation of different interleukin-1 receptor-associated kinase (IRAK) family members. *Mol. Cell* 11, 293–302.

2. Fujihara, M., Muroi, M., Tanamoto, K., Suzuki, T., Azuma, H., Ikeda, H. (2003) Molecular mechanisms of macrophage activation and deactivation by lipopolysaccharide: roles of the receptor complex. *Pharmacol. Ther.* **100**, 171–194.
3. Li, S., Strelow, A., Fontana, E. J., Wesche, H. (2002) IRAK-4: a novel member of the IRAK family with the properties of an IRAK-kinase. *Proc. Natl. Acad. Sci. USA* **99**, 5567–5572.
4. Cao, Z., Xiong, J., Takeuchi, M., Kurama, T., Goeddel, D. V. (1996) TRAF6 is a signal transducer for interleukin-1. *Nature* **383**, 443–446.
5. Burns, K., Janssens, S., Brissoni, B., Olivos, N., Beyaert, R., Tschopp, J. (2003) Inhibition of interleukin 1 receptor/Toll-like receptor signaling through the alternatively spliced, short form of MyD88 is due to its failure to recruit IRAK-4. *J. Exp. Med.* **197**, 263–268.
6. Muzio, M., Ni, J., Feng, P., Dixit, V. M. (1997) IRAK (Pelle) family member IRAK-2 and MyD88 as proximal mediators of IL-1 signaling. *Science* **278**, 1612–1615.
7. Ye, H., Arron, J. R., Lamothe, B., Cirilli, M., Kobayashi, T., Shevde, N. K., Segal, D., Dzivenu, O. K., Vologodskaia, M., Yim, M., Du, K., Singh, S., Pike, J. W., Darnay, B. G., Choi, Y., Wu, H. (2002) Distinct molecular mechanism for initiating TRAF6 signaling. *Nature* **418**, 443–447.
8. Li, X., Commane, M., Jiang, Z., Stark, G. R. (2001) IL-1-induced NFκB and c-Jun N-terminal kinase (JNK) activation diverge at IL-1 receptor-associated kinase (IRAK). *Proc. Natl. Acad. Sci. USA* **98**, 4461–4465.
9. Hayden, M. S., Ghosh, S. (2004) Signaling to NF-κB. *Genes Dev.* **18**, 2195–2224.
10. Chen, Z. J. (2005) Ubiquitin signaling in the NF-κB pathway. *Nat. Cell Biol.* **7**, 758–765.
11. Deng, L., Wang, C., Spencer, E., Yang, L., Braun, A., You, J., Slaughter, C., Pickart, C., Chen, Z. J. (2000) Activation of the IκB kinase complex by TRAF6 requires a dimeric ubiquitin-conjugating enzyme complex and a unique polyubiquitin chain. *Cell* **103**, 351–361.
12. Wang, C., Deng, L., Hong, M., Akkaraju, G. R., Inoue, J., Chen, Z. J. (2001) TAK1 is a ubiquitin-dependent kinase of MKK and IKK. *Nature* **412**, 346–351.
13. Baud, V., Liu, Z. G., Bennett, B., Suzuki, N., Xia, Y., Karin, M. (1999) Signaling by proinflammatory cytokines: oligomerization of TRAF2 and TRAF6 is sufficient for JNK and IKK activation and target gene induction via an amino-terminal effector domain. *Genes Dev.* **13**, 1297–1308.
14. Hirschfeld, M., Ma, Y., Weis, J. H., Vogel, S. N., Weis, J. J. (2000) Repurification of lipopolysaccharide eliminates signaling through both human and murine Toll-like receptor 2. *J. Immunol.* **165**, 618–622.
15. Sun, L., Deng, L., Ea, C. K., Xia, Z. P., Chen, Z. J. (2004) The TRAF6 ubiquitin ligase and TAK1 kinase mediate IKK activation by BCL10 and MALT1 in T lymphocytes. *Mol. Cell* **14**, 289–301.
16. Muroi, M., Ohnishi, T., Tanamoto, K. (2002) MD-2, a novel accessory molecule, is involved in species-specific actions of *Salmonella* lipid A. *Infect. Immun.* **70**, 3546–3550.
17. Muroi, M., Tanamoto, K. (2002) The polysaccharide portion plays an indispensable role in *Salmonella* lipopolysaccharide-induced activation of NF-κB through human Toll-like receptor 4. *Infect. Immun.* **70**, 6043–6047.
18. Kobayashi, N., Kadono, Y., Naito, A., Matsumoto, K., Yamamoto, T., Tanaka, S., Inoue, J. (2001) Segregation of TRAF6-mediated signaling pathways clarifies its role in osteoclastogenesis. *EMBO J.* **20**, 1271–1280.
19. Fukushima, T., Matsuzawa, S., Kress, C. L., Bruey, J. M., Krajewska, M., Lefebvre, S., Zapata, J. M., Ronai, Z., Reed, J. C. (2007) Ubiquitin-conjugating enzyme Ubc13 is a critical component of TNF receptor-associated factor (TRAF)-mediated inflammatory responses. *Proc. Natl. Acad. Sci. USA* **104**, 6371–6376.
20. Yamamoto, M., Okamoto, T., Takeda, K., Sato, S., Sanjo, H., Uematsu, S., Saitoh, T., Yamamoto, N., Sakurai, H., Ishii, K. J., Yamaoka, S., Kawai, T., Matsuura, Y., Takeuchi, O., Akira, S. (2006) Key function for the Ubc13 E2 ubiquitin-conjugating enzyme in immune receptor signaling. *Nat. Immunol.* **7**, 962–970.
21. Swantek, J. L., Tsen, M. F., Cobb, M. H., Thomas, J. A. (2000) IL-1 receptor-associated kinase modulates host responsiveness to endotoxin. *J. Immunol.* **164**, 4301–4306.
22. Kawagoe, T., Sato, S., Jung, A., Yamamoto, M., Matsui, K., Kato, H., Uematsu, S., Takeuchi, O., Akira, S. (2007) Essential role of IRAK-4 protein and its kinase activity in Toll-like receptor-mediated immune responses but not in TCR signaling. *J. Exp. Med.* **204**, 1013–1024.

Oral Microbiology Immunology 2008: 23: 60–69
Printed in Singapore. All rights reserved

ORAL MICROBIOLOGY
AND IMMUNOLOGY

Biological properties of the native and synthetic lipid A of *Porphyromonas gingivalis* lipopolysaccharide

H. Kumada[1], Y. Haishima[2], K. Watanabe[1], C. Hasegawa[2], T. Tsuchiya[2], K. Tanamoto[3], T. Umemoto[1]
[1]Department of Oral Microbiology, Kanagawa Dental College, Yokosuka, Kanagawa, Japan, [2]Divisions of Medical Devices, National Institute of Health Sciences, Setagaya, Tokyo, Japan, [3]Divisions of Microbiology, National Institute of Health Sciences, Setagaya, Tokyo, Japan

Kumada H, Haishima Y, Watanabe K, Hasegawa C, Tsuchiya T, Tanamoto K, Umemoto T. Biological properties of the native and synthetic lipid A of Porphyromonas gingivalis *lipopolysaccharide.*
Oral Microbiol Immunol 2008: 23: 60–69. © 2008 The Authors. Journal compilation © 2008 Blackwell Munksgaard.

Introduction and methods: A pentaacyl and diphosphoryl lipid A molecule found in the lipid A isolated from *Porphyromonas gingivalis* lipopolysaccharide (LPS) was chemically synthesized, and its characteristics were evaluated to reconfirm its interesting bioactivities including low endotoxicity and activity against LPS-unresponsive C3H/HeJ mouse cells.
Results: The synthesized *P. gingivalis* lipid A (synthetic Pg-LA) exhibited strong activities almost equivalent to those of *Escherichia coli*-type synthetic lipid A (compound 506) in all assays on LPS-responsive mice, and cells. LPS and native lipid A of *P. gingivalis* displayed overall endotoxic activities, but its potency was reduced in comparison to the synthetic analogs. In the assays using C3H/HeJ mouse cells, the LPS and native lipid A significantly stimulated splenocytes to cause mitosis, and peritoneal macrophages to induce tumor necrosis factor-α and interleukin-6 production. However, synthetic Pg-LA and compound 506 showed no activity on the LPS-unresponsive cells. Inhibition assays using some inhibitors including anti-human Toll-like receptor 2 (TLR2) and TLR4/MD-2 complex monoclonal antibodies showed that the biological activity of synthetic Pg-LA was mediated only through the TLR4 signaling pathway, which might act as a receptor for LPS, whereas TLR2, possibly together with CD14, was associated with the signaling cascade for LPS and native lipid A of *P. gingivalis*, in addition to the TLR4 pathway.
Conclusion: These results suggested that the moderated and reduced biological activity of *P. gingivalis* LPS and native lipid A, including their activity on C3H/HeJ mouse cells via the TLR2-mediated pathway, may be mediated by bioactive contaminants or low acylated molecules present in the native preparations having multiple lipid A moieties.

Key words: biological properties; lipopolysaccharide; *Porphyromonas gingivalis;* synthetic lipid A

Hidefumi Kumada, Department of Oral Microbiology, Kanagawa Dental College, 82 Inaoka-cho, Yokosuka, Kanagawa 238-8580, Japan
Tel./fax: +81 46 822 8867;
e-mail: kumadahi@kdcnet.ac.jp
Accepted for publication April 6, 2007

Porphyromonas gingivalis, an oral anaerobic gram-negative rod, is thought to be the most important mediator of the pathogenicity of periodontal disease (15, 47, 60). Many investigations have shown that the lipopolysaccharide (LPS) of *P. gingivalis* is a significant virulence factor, because it exhibits various activities, such as induction of inflammatory cytokines in human gingival fibroblast (HGF) cultures (12, 51) and bone resorption activity (18, 32), that are closely correlated with periodontal disease. *Porphyromonas gingivalis* LPS expresses a low level of endotoxic activity relative to enterobacterial LPS (29, 32). In addition, the LPS characteristically stimulates the splenocytes and macrophages from LPS-unresponsive C3H/HeJ mice

to cause mitosis or cytokine induction (8, 24, 59), in contrast to usual LPS, which do not exhibit any effects on these cells (43, 46).

The pathophysiological activity of LPS is dependent on the chemical structure of the hydrophobic portion, called lipid A, the biologically active center of LPS (16, 42). Recently, we found a characteristic structure of *P. gingivalis* lipid A containing branched and relatively longer fatty acids (15–17 carbon atoms) that are not present in enterobacterial lipid A molecules (26). In addition, we demonstrated, using LPS-antagonist and well-purified lipid A (although containing a small amount of protein), that the characteristic action of *P. gingivalis* lipid A against C3H/HeJ mice seems to be specifically mediated by the lipid A portion (54). These results suggested that the unique fatty acid components might be associated with the activity on C3H/HeJ mouse cells. This was also supported by studies of the chemical and biological properties of *Flavobacterium meningosepticum* lipid A, which has a structure very similar to *P. gingivalis* lipid A and also activates C3H/HeJ mouse cells (21, 56).

Toll, a *Drosophila* receptor molecule with extracellular leucine-rich repeats that currently has 10 published members [Toll-like receptors (TLRs) 1–10] in humans, has a role in triggering innate defenses against bacteria or fungi (1, 30, 52). Recent studies have suggested that TLR4, a member of the TLR family, might act as a receptor for LPS (4, 17, 39). TLR4 alone is not capable of sensing and signaling the presence of LPS, but another accessory molecule, MD-2, which is physically associated with TLR4, is required for LPS recognition through TLR4 (45). On the other hand, TLR2 has been proposed as a receptor for many microbial products and has been shown to signal the presence of peptidogylcan, lipoteichoic acid, lipoarabinomannan, lipoproteins and lipopeptides, as well as many whole gram-positive bacteria (4, 53). In addition, it has been reported that the co-dominant LPS^d allele of C3H/HeJ mice corresponds to a missense mutation in the third exon of the *TLR4* gene, which is predicted to result in replacement of proline with histidine at position 712 of the protein (39). Recently, we found that HGFs constitutively express *TLR2* and *TLR4*, and that their levels of expression are increased by stimulation with *P. gingivalis* LPS (50). These observations suggest that, in addition to TLR4, the biological action of *P. gingivalis* LPS may be mediated through the TLR2 pathway, which might not be correlated with LPS-mediated signaling.

In the present study, we chemically synthesized a pentaacyl and diphosphoryl lipid A analog corresponding to the lipid A species with the highest molecular mass found in *P. gingivalis* native lipid A in our previous study (26). The synthetic analog was subjected to biological assay to evaluate whether the interesting activity of LPS against C3H/HeJ mice is derived from the lipid A part.

Materials and methods

Reagents

RNase A, DNase I, and proteinase K were purchased from Sigma (St Louis, MO). (*R,S*)-3-hydroxy-13-methyltetradecanoic acid (3-OH-iC$_{15:0}$), (*R,S*)-3-hydroxy-15-methylhexadecanoic acid (3-OH-iC$_{17:0}$) and (*R,S*)-3-hydroxyhexadecanoic acid (3-OH-C$_{16:0}$) were purchased from Iatron-Biosupply Co. (Tokyo, Japan) and Wako Chemical Co. (Osaka, Japan). Quantitative *Limulus* amebocyte lysate (LAL) gelation assay reagent, Endospecy, was obtained from Seikagaku Kogyo (Tokyo, Japan). Iscove's modified Dulbecco and RPMI-1640 media were the obtained from Life Technologies (Grand Island, NY) and Gibco Laboratories (Grand Island, NY). [^{3}H]Thymidine was obtained from New England Nuclear (Boston, MA). Mono-Mac-6 (MM6) cells were purchased from the German Collection of Microorganisms and Cell Cultures (Braunschweig, Germany). HTA125, TL2.1, and MY4 clones, monoclonal antibodies (mAbs) to the human TLR4/MD-2 complex, and human TLR2 and CD14 molecules were purchased from MBL Medical & Biological Laboratories Co. (Nagoya, Japan), Cascade BioScience, (Winchester, MA) and Coulter Co. (Miami, FL), respectively.

Microbes

P. gingivalis SU63, isolated from a periodontal pocket, was grown anaerobically at 37°C for 24 h in heart infusion broth (Difco Laboratories, Detroit, MI) supplemented with 0.0005% hemin, 0.0001% vitamin K1, 0.5% yeast extract, and 0.08% cysteine (25). The cells were heated (121°C for 15 min), harvested by centrifugation (7000 *g*, 20 min), and washed successively with distilled water and acetone.

Animals

Japanese White rabbits were purchased from Japan SLC, Inc. (Hamamatsu, Japan). Female C3H/HeN and C3H/HeJ mice aged 6 weeks were obtained from Clea Japan, Inc. (Tokyo, Japan), and used for the assay of splenic mitogenicity and the induction of tumor necrosis factor-α (TNF-α) and interleukin-6 (IL-6) by peritoneal macrophages.

Preparations of *P. gingivalis* LPS and lipid A

The procedures for the preparation of *P. gingivalis* LPS and lipid A were described previously (26). Briefly, the LPS was extracted from acetone-dried cells with phenol–water (58), digested with RNase A, DNase I, and proteinase K (44), and then purified by repeated ultracentrifugation (105,000 *g*, 12 h, six times). The LPS was washed successively with phenol/chloroform/petroleum ether [2 : 5 : 8, volume/volume (V/V)] (10) and acetone and then lyophilized.

The free lipid A was recovered from hydrolysates (1% acetic acids, 100°C, 1.5 h) of LPS according to the methods of Qureshi et al. (40, 41). It was purified by passage through a Dowex 50 (H^+) column with chloroform/methanol (3 : 1, V/V) as the eluent and gel permeation chromatography with a Sephadex LH-20 (Pharmacia, Uppsala, Sweden) column with the same solvent as the eluent (26).

Total synthesis of *P. gingivalis* SU63 lipid A

P. gingivalis lipid A analog (compound 1) (Fig. 1) was synthesized basically according to the procedure previously reported (26). As shown in Fig. 2, (*R,S*)-3-OH-iC$_{15:0}$, (*R,S*)-3-OH-iC$_{17:0}$ and (*R,S*)-3-OH-C$_{16:0}$ were selectively (*S*)-3-*O*-acetylated by lipase treatment (5) of the methyl esters. The non-acetylated methyl esters predominantly containing the (*R*)-forms were separated by silica-gel chromatography, and each free acid was fractionally crystallized from CH_3CN as the dibenzylamine salt to increase the percentage of enantiomorphic excess. The optically pure (*R*)-3-OH fatty acids (compounds 2–4) were converted to the phenacyl ester (compounds 5–7) and 3-*O*-acylated with C$_{16:0}$ or benzyloxycarbonyl chloride (Z-Cl) to obtain the phenacyl ester of (*R*)-3-*O*-Z-iC$_{15:0}$ (compound 8), (*R*)-3-*O*-Z-C$_{16:0}$ (compound 9), (*R*)-3-*O*-Z-iC$_{17:0}$ (coumpound 10) and (*R*)-3-*O*-(hexadecanoyl)-15-methylhexadecanoic acid [3-*O*-(C$_{16:0}$)-iC$_{17:0}$] (compound 11). After dephenacylation, each fatty acid (compounds 12–15) was purified by silica-gel chromatography, and the yields of

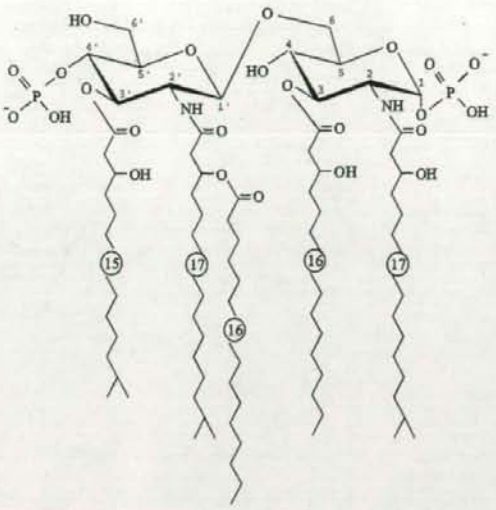

Fig. 1. Chemical structure of *Porphyromonas gingivalis* synthetic lipid A. In this study, we chemically synthesized a pentaacyl and diphosphoryl lipid A analog corresponding to the lipid A species with the highest molecular mass found in *P. gingivalis* native lipid A in our previous study (26). The synthetic Pg-LA consists of β(1-6)-linked D-glucosamine disaccharide 1,4′-bisphosphate backbone acylated with (*R*)-3-OH-$iC_{17:0}$, (*R*)-3-OH-$C_{16:0}$, (*R*)-3-OH-($C_{16:0}$)-$iC_{17:0}$ and (*R*)-3-OH-$iC_{15:0}$ at positions 2, 3, 2′ and 3′ of the hydrophilic backbone.

compounds 12–14 were 8.9%, 24.1%, and 9.7%, respectively.

The glycosyl donors were prepared from *N*-(2,2,2-trichloroethoxycarbonyl)-D-gluco samine (compound 16) as shown in FIG. 3. After allyl glycosidation, isopropylidenation of the glycoside followed by simple recrystallization afforded almost pure 4,6-*O*-isopropylidenated α-allyl glycoside, compound 17. This product was 3-*O*-acylated with (*R*)-3-*O*-*Z*-$iC_{15:0}$ to obtain compound 18, and the 4,6-*O*-protection was removed by mild acid hydrolysis to give product 19. Position 6 of the compound was protected with a carbobenzoxyl group to synthesize compound 20 followed by 4-*O*-diphenylphosphorylation (compound 21) and subsequent cleavage of the allyl group to make compound 22 (33, 38). This product was allowed to react with CCl_3CN in the presence of Cs_2CO_3 (57) as a catalyst to give glycosyl trichloroacetimidate, compound 23, to be used as the donor.

On the other hand, glycosyl acceptor was prepared through compound 17 (Fig. 4). The compound was 3-*O*-acylated with (*R*)-3-*O*-*Z*-$C_{16:0}$ to obtain compound 24. After removing the Troc group, the product 25 was *N*-acylated with (*R*)-3-*O*-*Z*-$iC_{17:0}$ to give compound 26 followed by cleavage of the 4,6-*O*-protection to yield glycosyl acceptor 27. Coupling reaction of compound 23 with 27 was performed using trimethylsilyl triflate (TMSOTf) in 1,2-dichloroethane to obtain disaccharide 28, which gave the desired β(1 → 6) linkage in a higher yield than the Königs–Knorr and oxazoline methods (9, 19). After removing the Troc group of the disaccharide compound, the 2′-amino group of product 29 was *N*-acylated with (*R*)-3-*O*-($C_{16:0}$)-$iC_{17:0}$ to prepare compound 30. Compound 31 with a free 1-hydroxyl group was prepared by cleavage of the allyl group, and then 1α-*O*-phosphorylation to yield the protected 1,4′-bisphosphate compound 32 was performed by 1-*O*-lithiation with buthyllithium (BuLi) and subsequent treatment with tetrabenzyl diphosphate (9, 19, 20). The product purified using silica-gel chromatography was deprotected by two-step hydrogenolysis (8 kg/cm^2 of H_2) with Pd-black in THF and subsequent platinum

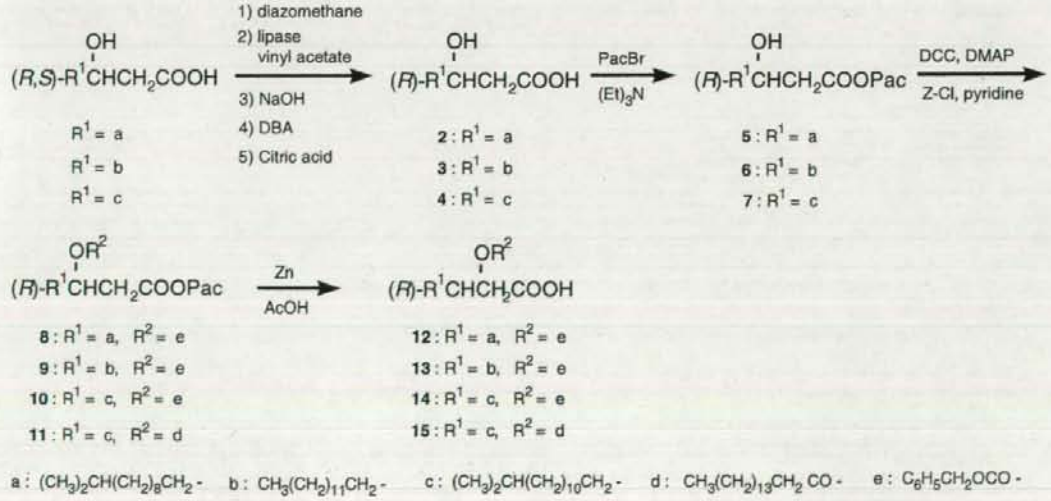

Fig. 2. Synthesis of (*R*)-3-hydroxy fatty acids; (*R*)-3-OH-$iC_{15:0}$, (*R*)-3-OH-$C_{16:0}$, (*R*)-3-OH-$iC_{17:0}$ and (*R*)-3-OH-($C_{16:0}$)-$iC_{17:0}$. Synthetic procedures of each fatty acid are described in the Materials and methods.

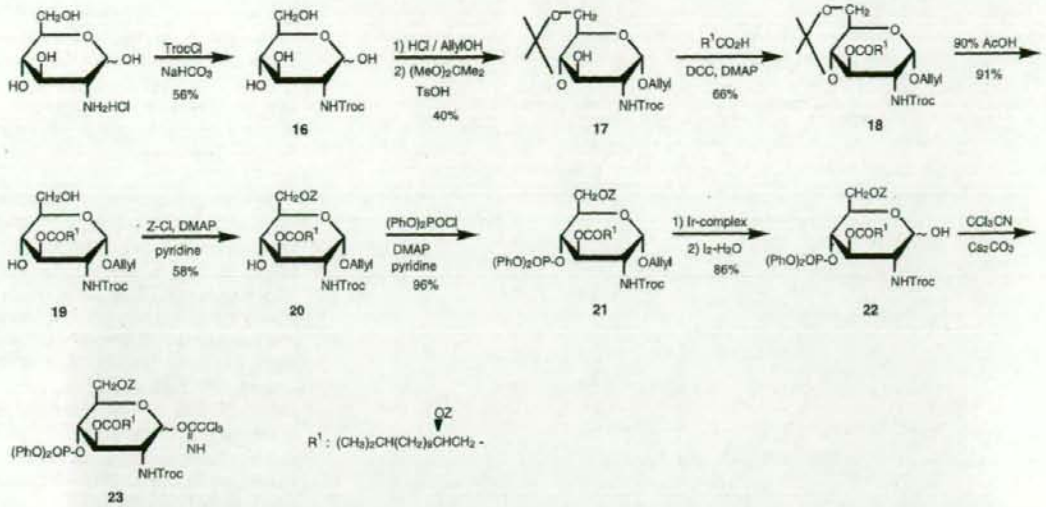

Fig. 3. Total synthesis of *Porphyromonas gingivalis* lipid A (step 1). Step 1 was performed for the preparation of a glycosyl donor corresponding to the terminal residue. Synthetic procedures of step 1 are described in the Materials and methods.

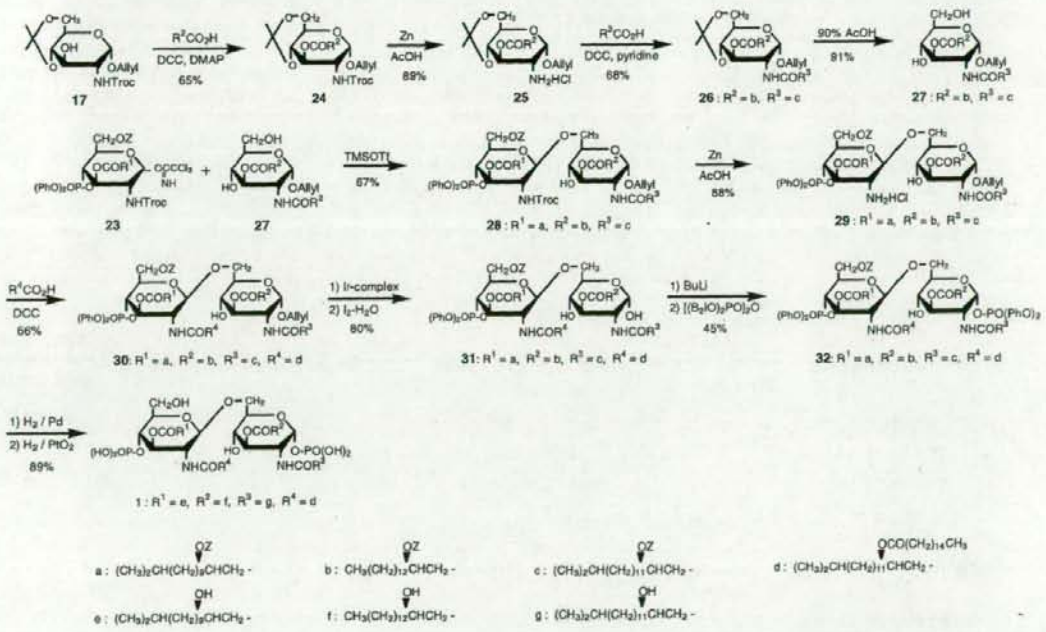

Fig. 4. Total synthesis of *Porphyromonas gingivalis* lipid A (step 2). Step 2 involved the preparation of a glycosyl acceptor corresponding to a non-terminal residue and coupling reaction of each unit. Synthetic procedures of step 2 are described in the Materials and methods.

oxide (PtO_2) in THF-H_2O (20 : 1) to give a good yield of *P. gingivalis* lipid A analog (compound 1), synthetic *P. gingivalis* lipid A (Pg-LA). Finally, the analog was effectively purified by centrifugal partition chromatography (49) using $CHCl_3$-MeOH-iPrOH-H_2O-Et_3N = 20 : 20 : 2.5 : 22.5 : 0.01 as a two-phase eluate on a Model LLB-M instrument (Sanki Engineering Ltd., Kyoto, Japan). The structure was confirmed by liquid secondary ion-mass spectrometry (m/z 1768.2 $[M-H]^-$) in negative ion mode and by nuclear magnetic resonance spectroscopy, which demonstrated

β-configuration of the glycosidic linkage, linkage positions of phosphate groups (1 and 4'), and α-configuration of the phosphorylated position 1.

Liquid secondary ion-mass spectrometry and nuclear magnetic resonance spectroscopy

Both liquid secondary ion-mass spectrometry and nuclear magnetic resonance spectroscopy were performed according to the methods reported previously (26).

LAL gelation assay

LAL gelation activity was measured by the chromogenic endotoxin-specific assay, Endospecy, using recombinant *Limulus* coagulation enzyme from horseshoe crab (34). Aliquots of 50-μl samples were incubated with the same volume of lysate containing chromogenic substrate in 96-well flat microplates at 37°C for 30 min. The absorbance was measured with a microplate reader (Wellreader SK-601, Seikagaku Kogyo) at 405 and 492 nm simultaneously, the latter as a reference. The data were expressed as the Δ absorbance (405–492 nm) per minute [ΔAbs/min (405–492 nm)].

Schwartzman assay

As described previously (27), the dermal Schwartzman assay was performed by injecting three male Japanese White rabbits (1.5–2.0 kg) intradermally into the shaved abdomen with 1, 10, or 100 μg of samples in 0.1 ml Dulbecco's phosphate buffered saline (PBS) (Nissui Pharmaceutical Co., Tokyo, Japan), followed 24 h later by a challenge intravenous injection of 100 μg *Salmonella typhimurium* LPS (Sigma) in 0.1 ml Dulbecco's PBS. The injection sites were examined for hemorrhagic necrosis 5 h after injection of the challenge dose. The results were expressed as the minimum dose of each sample to cause a hemorrhagic necrosis spot over 0.5 mm in diameter at the injection site.

Mitogenicity assay

Mitogenic activity was examined by the incorporation of [^{3}H]thymidine into spleen cells from C3H/HeN and C3H/HeJ mice as described (54). Mouse spleen cells were suspended in serum-free Iscove's modified Dulbecco's medium and washed with the same medium. The cells (8×10^5 cells/0.2 ml/well) were cultured in 96-well microplates containing various amounts of samples for 72 h at 37°C in a humidified 5% CO_2 atmosphere. During the final 24 h, 0.5 mCi (18.5 kBq) of [^{3}H]thymidine (18.2 Ci/mmol) per well was added and the incorporation of [^{3}H]thymidine by the cultured cells was measured with a liquid scintillation counter. The results were expressed as mean counts per minute (c.p.m.) of triplicate determinations.

Stimulation of murine macrophages and HGFs

Mouse peritoneal macrophages were obtained from C3H/HeN and C3H/HeJ mice injected intraperitoneally with 3.0 ml thioglycollate medium. The peritoneal cells (1×10^6 cells/ml), suspended in serum-free RPMI medium, were incubated for 2 h at 37°C in a humidified 5% CO_2 atmosphere. After incubation, adherent cells were stimulated for 47 h with samples to induce TNF-α and IL-6 production, and then the cell-free supernatants, passed through 0.22-μm Millex filters (Millipore Co., Bedford, MA), were stored at –20°C until used for the assays.

Normal HGFs obtained from patients were established by the explant growth method from clinically healthy gingival tissues as described elsewhere (61). The HGFs from passage 5 to 12 were cultured in Dulbecco's modified Eagle's medium (Nissui Pharmaceutical Co.) containing 10% fetal calf serum (Gibco), penicillin (100 U/ml), and streptomycin (100 μg/ml) under 5% CO_2. After incubation for 4 days, the fibroblast layers were washed twice with Dulbecco's modified Eagle's medium and then incubated with 1 μg/ml of each sample without fetal calf serum for 47 h. The cell-free supernatants were harvested and stored at –20°C until used for the assays.

Cytokine assays

TNF-α and IL-6 activity in murine–macrophage culture supernatants were determined in duplicate using an enzyme-linked immunosorbent assay (ELISA) kit (Genzyme Co., Cambridge, MA), respectively.

TNF-α production was assayed using clone MM6-CA8 derived from Mono-Mac-6 (MM6) cells, a human monocytoid cell line with high sensitivity to LPS stimulation (48). MM6-CA8 cells exhibit a superior response to low concentrations of endotoxin and peptidogylcan in producing proinflammatory cytokines. MM6-CA8 cells were cultured in RPMI-1640 medium containing fetal bovine serum (10%), glutamine (2 mM), non-essential amino acids (0.1 mM), sodium pyruvate (1 mM) and bovine insulin (9 μg/ml). After cell priming (72 h) with calcitriol (1,25-dihydroxy-vitamin D3), the cells (1×10^6 cells ; 0.9 ml/well) were seeded in 24-well plates, and various dilutions (0.1 ml) of sample were added. After incubation for 17 h, TNF-α released into the culture supernatants was immunoenzymatically measured using commercial ELISA kits as described above.

Inhibition assays

To examine the effects of polymyxin B and mAb to CD14 on the production of IL-8, 100 U/ml of polymyxin B sulfate (Sigma) and 2.5 μg/ml anti-CD14 (MY4, Coulter Co., Miami, FL) was added simultaneously or after pretreatment for 2 h, respectively, to the HGF cultures stimulated with 1 μg/ml of samples for 47 h. The production of IL-8 from HGFs was determined in duplicate using a human IL-8 ELISA kit (Amersham, Piscataway, NJ).

For the inhibition assay of TNF-α from MM6-CA8 cells, 5 μg/ml anti-human TLR2 and TLR4/MD-2 complex mAbs, and 10 μg/ml anti-human CD14 were added to MM6-CA8 cell suspension in 24-well plates, and after 1 h, each sample (10 ng/ml native lipid A, and 1 ng/ml synthetic Pg-LA and 506) was added to the cell suspension. After incubation, TNF-α production by the cells was measured.

Results

LAL gelation activity

The LAL gelation activity of each sample was estimated by the kinetic-chromogenic assay using LPS-specific reagent. As shown in Fig. 5, the activity increased in a dose-dependent manner over the range of concentrations tested (1 pg/ml to 1 μg/ml). Synthetic Pg-LA exhibited strong LAL gelation activity equivalent to that of compound 506, which was used as a control. On the other hand, LAL activities of *P. gingivalis* LPS and native lipid A, reported previously as a weakly toxic endotoxin (55), were approximately 10,000-fold or 100-fold weaker than that of compound 506, respectively.

Schwartzman reaction

Localized Schwartzman activity in rabbits was measured, and the results are shown in Table 1. *S. typhimurium* LPS and compound 506, used as positive controls, exhibited strong activity, and the minimum doses to induce a Schwartzman reaction of

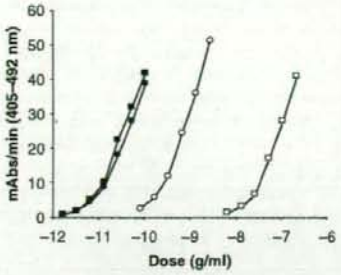

Fig. 5. LAL gelation activity of *Porphyromonas gingivalis* synthetic lipid A. LAL gelation activity was estimated by the kinetic-chromogenic assay using the LPS-specific reagent, Endospecy. Fifty-microliter aliquots of samples were incubated with the same volume of lysate at 37°C for 30 min. The data are expressed as the Δ absorbance (405–492 nm) per minute [ΔAbs/min (405–492 nm)]. ●, synthetic Pg-LA; ○, native lipid A; □, LPS; ■, compound 506.

each sample were 5 and 10 μg/site, respectively. Schwartzman activity of synthetic Pg-LA was similar to that of these positive controls, and the minimum inducing dose was 10 μg/site. However, minimum inducing doses of *P. gingivalis* LPS and native lipid A were 100 and 50 μg/site, respectively.

Mitogenicity

The mitogenic activities of samples were tested on murine splenic cells from LPS-responsive C3H/HeN and LPS-unresponsive C3H/HeJ mice. As shown in Fig. 6A, synthetic Pg-LA and compound 506 showed activity in response to splenic cells from C3H/HeN mice even at a dose of 1 μg/ml, and the activity increased in a dose-dependent manner over the dose range tested. *P. gingivalis* native lipid A also exhibited activity similar to those of both synthetic compounds. As shown in Fig. 6B, significant mitogenicity was observed in the splenic cells from LPS-unresponsive C3H/HeJ mice treated with

Table 1. Minimum dose of *Porphyromonas gingivalis* synthetic lipid A inducing a local Schwartzman reaction

Stimulants	Minimum inducing dose (μg/site)
P. gingivalis	
synthetic lipid A	10
native lipid A	50
LPS	100
Compound 506	
S. typhimurium	5

The minimum dose of samples for positive reaction was determined as the amount inducing a hemorrhagic spot more than 0.5 mm in diameter.

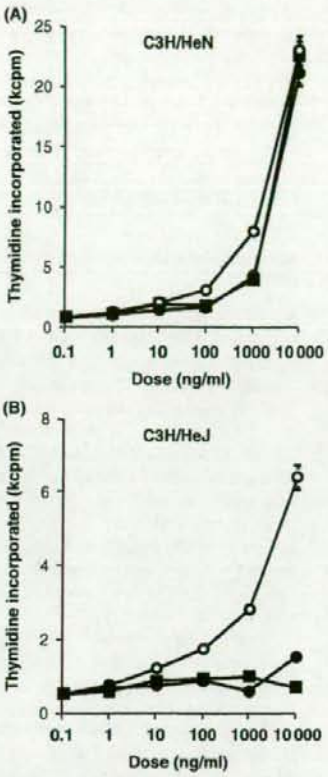

Fig. 6. Mitogenic responses of murine spleen cells from C3H/HeN and C3H/HeJ mice to *Porphyromonas gingivalis* synthetic lipid A. Spleen cells (8×10^5 cells/0.2 ml) were cultured in 96-well microplates containing various amounts of samples for 72 h. During the final 24 h, 0.5 mCi (18.5 kBq) of [^{3}H]thymidine (18.2 Ci/mmol) per well was added. The results are expressed as mean c.p.m. ± SD of triplicate experiments. ●, synthetic Pg-LA; ○, native lipid A; ■, compound 506.

P. gingivalis native lipid A, whereas synthetic Pg-LA and control compound 506 had no mitogenic activity even at a concentration of 10 μg/ml.

Induction of inflammatory cytokine release from various cells

Cytokine production by lipid A stimulation was assayed using HGFs, peritoneal macrophages from C3H/HeN and C3H/HeJ mice, and human MM6-CA8 cells. As shown in Table 2, native lipid A and synthetic Pg-LA exhibited activity for IL-8 induction activity in HGFs that was similar to that of compound 506 (1132.6, 1085 and 1056.9 pg/ml, respectively). The activity of synthetic analogs was significantly inhibited by polymyxin B and anti-CD14 mAb, whereas that of native lipid A was not inhibited by polymyxin B and anti-human CD14 mAb reduced the activity by only 50%.

Synthetic compound 506, used as a control, exhibited strong TNF-α and IL-6 induction in thioglycollate-elicited peritoneal macrophages from LPS-responsive C3H/HeN mice at doses of <10 ng/ml, as shown in Figs 7A and 8A. The activities of *P. gingivalis* synthetic and native lipid A were approximately 10- to 100-fold weaker than those of compound 506, respectively (Figs 7A and 8A). The *P. gingivalis* native lipid A significantly stimulated TNF-α and IL-6 production in peritoneal macrophages from LPS-unresponsive C3H/HeJ mice (Figs 7B and 8B). These LPS-unresponsive mice showed a similar minimum lipid A stimulatory dose and similar levels of cytokine production to C3H/HeN mice (Figs 7A and 8A). However, no induction of TNF-α or IL-6 release was observed with synthetic Pg-LA and compound 506, as shown in Figs 7B and 8B.

As shown in Table 3, synthetic Pg-LA and compound 506 stimulated TNF-α production in human monocytoid MM6-CA8 cells even at a low dose (each 1 ng/ml), whereas moderate activity in the cells was observed by native lipid A (10 ng/ml). Anti-human TLR4/MD-2 complex mAb significantly blocked the TNF-α production by synthetic Pg-LA and compound 506, whereas 7% inhibition and 6% inhibition were observed by anti-human TLR2 mAb (Table 3). On the other hand, both anti-human TLR2 and TLR4/MD-2 complex mAbs were essential to suppress cytokine production by *P. gingivalis* native lipid A (Table 3). In addition, anti-human CD14 mAb also completely inhibited TNF-α production induced by synthetic Pg-LA and compound 506, but approximately 70% inhibition was observed by native lipid A, as well as the results of the IL-8 production from HGF cells (Table 2).

Discussion

In the present study, we synthesized an analog of *P. gingivalis* lipid A according to the chemical structure proposed in our previous report (26), to reconfirm the biological data reported to date by some investigators using LPS or native lipid A (8, 24, 50, 54, 55, 59), including its action on C3H/HeJ mice. Some reports suggested that *P. gingivalis* LPS possesses lipid A structural heterogeneity, consisting of only a tri-acylated monophosphorylated form (37), and of a multiple heterogeneity